# WEAKLY IMPLICIT NUMERICAL SCHEMES FOR THE TWO-FLUID MODEL

STEINAR EVJE[A,C] AND TORE FLATTEN[B]

Abstract. The aim of this paper is to construct semi-implicit numerical schemes for a two-phase (two-fluid) flow model, allowing for violation of the CFL-criterion for sonic waves while maintaining a high level of accuracy and stability on volume fraction waves. Based on the results of a previous work [12], we here present a general framework for constructing such *weakly implicit* schemes without making use of any Riemann solver nor referring to any calculation of flux jacobians.

One important step of the proposed methods is the introduction of a pressure evolution equation. This equation, which is discretized at cell-interfaces, naturally defines a consistent numerical flux for the discretization of the pressure term of the two momentum equations. This step is crucial for the stability of the solutions when the CFL-criterion for sonic waves is violated. Another major step is the decomposition of the numerical mass fluxes $F_k$, corresponding to the physical mass flux $f_k = \rho_k \alpha_k v_k$, into two components $F_k^D$ and $F_k^A$ respectively. The purpose of the $F_k^D$-component is to ensure stability (non-oscillatory behavior) of solutions when the time step is dictated by the fluid velocity and not the sonic velocity, whereas the $F_k^A$-component is designed such that accurate resolution of volume fraction waves is ensured. Our techniques, which we refer to as "Mixture Flux" (MF) methods, are based on the above two steps, but give room for different choices in the discretization of the pressure evolution equation as well as the construction of the $F_k^D$ and $F_k^A$ flux components. Particularly, by using an AUSMD type of discretization for the $F_k^A$-component (originally proposed for the Euler equtions in [32]) we obtain a Weakly Implicit Mixture Flux AUSMD scheme.

We present several numerical simulations, all of them indicating that the CFL-stability of the resulting WIMF-AUSMD scheme is largely governed by the velocity of the volume fraction waves and not the rapid sonic waves. Comparisons with an explicit Roe scheme indicate that the scheme presented in this paper is highly efficient, robust and accurate on slow transients. In fact, by exploiting the possibility to take much larger time steps it outperforms the Roe scheme in the resolution of the volume fraction wave for the classical water faucet problem. On the other hand it is more diffusive on pressure waves. Although conservation of positivity for the masses is not proven, we demonstrate that a transition fix may be applied making the scheme able to handle transition to one-phase flow while maintaining a high level of accuracy on volume fraction fronts.

**subject classification.** 76T10, 76N10, 65M12, 35L65

**key words.** two-phase flow, two-fluid model, hyperbolic system of conservation laws, flux splitting, implicit scheme

## 1. Introduction

Accurate resolution of the dynamics related to two-phase flow phenomena is of high importance for a number of engineering applications, including nuclear reactor safety analysis and petroleum engineering. Among several two-phase flow models there are two fundamentally different formulations of the macroscopic field equations; namely the *two-fluid* model and the *mixture* model [26]. Here we focus on the two-fluid model. This is considered to give the most general and detailed description of transient two-phase flows. In the two-fluid model each phase is treated separately

*Date*: August 7, 2003.

[A]RF-Rogaland Research, Prof. Olav Hanssensvei 15, Stavanger, Norway.

[B]Department of Energy and Process Engineering, Norwegian University of Science and Technology, Kolbjorn Hejes vei 1B, N-7491, Trondheim, Norway.

Email: steinar.evje@rf.no, tore.flatten@maskin.ntnu.no.

[C]Corresponding author.

in terms of two sets of conservation equations; one for each phase. The interaction terms between the two phases appear in the basic equations as transfer terms across the interfaces (source terms). More precisely, the basic form of the model can be written on the following vector form:

$$\partial_t \begin{pmatrix} \rho_{\mathrm{g}}\alpha_{\mathrm{g}} \\ \rho_{\mathrm{l}}\alpha_{\mathrm{l}} \\ \rho_{\mathrm{g}}\alpha_{\mathrm{g}}v_{\mathrm{g}} \\ \rho_{\mathrm{l}}\alpha_{\mathrm{l}}v_{\mathrm{l}} \end{pmatrix} + \partial_x \begin{pmatrix} \rho_{\mathrm{g}}\alpha_{\mathrm{g}}v_g \\ \rho_{\mathrm{l}}\alpha_{\mathrm{l}}v_l \\ \rho_{\mathrm{g}}\alpha_{\mathrm{g}}v_g^2 + \alpha_g p \\ \rho_{\mathrm{l}}\alpha_{\mathrm{l}}v_l^2 + \alpha_l p \end{pmatrix} = \begin{pmatrix} 0 \\ 0 \\ p\partial_x\alpha_g + \tau_g \\ p\partial_x\alpha_l + \tau_l \end{pmatrix} + \begin{pmatrix} 0 \\ 0 \\ Q_g + M_g^D \\ Q_l + M_l^D \end{pmatrix}. \tag{1}$$

Here $\alpha_k$ is the volume fraction of phase $k$ with $\alpha_l + \alpha_g = 1$, $\rho_k$ and $v_k$ denote the density and fluid velocities of phase $k$, and $p$ is the pressure common to both phases. Moreover, $\tau_k$ represents the interfacial forces which contain differential terms (hence, is relevant for the hyperbolicity of the model) and satisfy $\tau_g + \tau_l = 0$. $M_k^D$ represents interfacial drag force with $M_g^D + M_l^D = 0$ whereas $Q_k$ represent source terms due to gravity, friction, etc.

The model we will be concerned with is classified as a hyperbolic set of differential equations, with the implication that information flows in the system along characteristic curves with a certain velocity. For such models *explicit* numerical schemes are commonly used, advantage being taken of the fact that the time development of the state at some point depends only on points within the span of the characteristic curves in time and space. Explicit schemes are simple to implement and may give more flexibility in the treatment of complex pipe networks. However, they are subject to the CFL constraint

$$\frac{\Delta x}{\Delta t} \geq |\lambda_{\max}| \tag{2}$$

where $\lambda_{\max}$ is the largest eigenvalue for the system. For the two-fluid model we are concerned with, the four eigenvalues are pairwise associated with sonic and volume fraction waves [9]. The sonic waves may be several orders of magnitude faster than the volume fraction waves, although the latter may often be of greater interest to the researcher. For this reason the CFL criterion (2) may severely limit the computational efficiency of explicit schemes.

To remedy the situation, a step in a more implicit direction, i.e. coupling one or more variables throughout the computational domain, may be made. Such approaches may be classified as follows:

- *Weakly implicit.* The original CFL criterion (2) may be broken for sonic waves, but a weaker CFL criterion for volume fraction waves still applies

$$\frac{\Delta x}{\Delta t} \geq |\lambda_{\max}^{\mathrm{v}}|, \tag{3}$$

  where $\lambda_{\max}^{\mathrm{v}}$ is the largest of the two eigenvalues corresponding to volume fraction waves.
- *Strongly implicit.* No CFL-like stability criterion applies and the equations may be integrated with arbitrary timestep. However, stability could still be affected by other issues such as inherent stiffness of the equations.

The majority of engineering computer software for two-fluid simulations seems to be based on some implicit approach. Examples include the CATHARE code [2] developed for the nuclear industry, and OLGA [3] aimed towards the petroleum industry. The recently developed PeTra [13] is largely based on the OLGA approach, being strongly implicit in the sense of the classification above. On the other hand, the TACITE code [21] was originally based on an explicit approach.

Trapp and Riemke [31] describe some of the earlier computer simulation tools for two-phase flow. It seems to be long known that a weak pressure-momentum coupling may be enough to break the sonic CFL-criterion, making the scheme weakly implicit in the sense of the classification above. However, due to the lack of computer power even weakly implicit schemes were often too inefficient and strongly implicit schemes were favored in the early days. In addition, most early schemes where based on upwinding based on the advective velocities, and the effect of sonic waves was not naturally integrated in the discretization. Such advective splitting schemes are intrinsically unstable and a staggered donor-cell approach was typically needed to stabilize the numerical solution. This lack of stability seems also to have been a motivation in moving from weakly to the more stable strongly implicit schemes.

In recent years there has been several new applications of different upwind techniques for the equations of two-phase flow. Examples include implementations of the Roe scheme by Toumi et

al [30, 29, 5], Romate [23], Tiselj and Petelin [27], Fjelde and Karlsen [11]. A rough Godunov scheme was implemented by Masella et al [17]. Coquel et al [4] studied kinetic upwind schemes, which do not make use of the eigenstructure, for the approximation of a general two-fluid model. Saurel and Abgrall have studied a general compressible unconditionally hyperbolic two-phase model with a wide range of applications, see [24, 25].

For one-phase flow, Wada and Liou [32] suggested a hybrid flux difference splitting (FDS) and flux vector splitting (FVS) scheme with good accuracy and stability properties. Their idea has been extended to two-phase flow models by Edwards et al [6], Niu [18, 19], and Evje et al [7, 8, 9].

Based on these recent results and the rapid development of computer speed we believe that weakly implicit schemes may provide several advantages compared to strongly implicit or explicit schemes. This is based on the following considerations:

- *Efficiency.* Many industrial applications require that simulations must be performed in real time, for instance if the numerical model is used to produce input to an automatic choke controller. This limits the applicability of explicit schemes due to the strict CFL criterion (2). However, computers are now so fast that timesteps below the volume fraction CFL criterion (3) may give real time performance.
- *Robustness.* Modern discretization techniques are more robust, implicating that the difference in stability between weakly and strongly implicit schemes may not be significant.
- *Accuracy.* As opposed to strongly implicit schemes, weakly implicit schemes more easily allow for high resolution methods like the MUSCL approach of van Leer [14] to achieve improved accuracy on the volume fraction waves.

A weakly implicit numerical scheme for the mixture model has been presented by Faille and Heinze [10]. They used a rough finite volume method based on an eigenvalue decomposition of the jacobi matrix for the system. A weakly implicit scheme for the two-fluid model was studied by Masella et al [16].

The aim of this work is to develop a general methodology for constructing numerical schemes for the two-fluid model which possesses the following important properties:

- No use of riemann solver or computation of nonlinear flux jacobians;
- Accurate and non-oscillatory resolution of mass fronts, i.e. slow-moving volume fraction waves, comparable with the resolution given by upwind type of schemes like the Roe scheme;
- Stability under the weak CFL condition (3).

We first describe the discretization procedure in a general semi-discrete setting where a system of ODEs replaces the continuous model (1). A special feature of the proposed method is that we systematically make use of the following pressure evolution equation (see Section 2 for details)

$$\frac{\partial p}{\partial t} + \kappa \left( \rho_{\mathrm{l}} \frac{\partial}{\partial x} \left( \rho_{\mathrm{g}} \alpha_{\mathrm{g}} v_{\mathrm{g}} \right) + \rho_{\mathrm{g}} \frac{\partial}{\partial x} \left( \rho_{\mathrm{l}} \alpha_{\mathrm{l}} v_{\mathrm{l}} \right) \right) = 0 \tag{4}$$

where

$$\kappa = \frac{1}{\frac{\partial \rho_{\mathrm{l}}}{\partial p} \alpha_{\mathrm{l}} \rho_{\mathrm{g}} + \frac{\partial \rho_{\mathrm{g}}}{\partial p} \alpha_{\mathrm{g}} \rho_{\mathrm{l}}}. \tag{5}$$

The main mechanism of the proposed semi-discrete scheme can be described by the following two steps:

(I) The pressure calculation is coupled to the momentum equations. This is achieved by discretizing (4) at the cell interface $j + 1/2$. We then directly obtain a numerical flux for the pressure term of the momentum equations which is consistent with the model under considerations. This turns out to be an essential step in order to redeem the scheme from the strong CFL condition (2).

(II) As regards the mass conservation equations, we introduce a decomposition of the numerical mass fluxes $F_k$, which is an approximation to the physical mass flux $f_k = \rho_k \alpha_k v_k$, into two components $F_k^D$ and $F_k^A$ respectively. The purpose of the $F_k^D$-component is to couple the mass and momentum equations in a consistent manner and thereby ensure that the scheme yields stable mass calculations also for timesteps dictated by the weak CFL condition (3).

The purpose of the $F_k^A$ component is to ensure that accurate resolution of volume fraction waves is obtained.

Our techniques, represented by the above two steps, will be referred to as "Mixture Flux" (MF) methods. A delicate issue is to derive an appropriate balancing of the two components $F_k^D$ and $F_k^A$ in the formulation of the numerical mass fluxes $F_k$. This balancing is achieved by systematically using the important relation

$$\frac{m_{\rm g}}{\rho_{\rm g}(p)} + \frac{m_{\rm l}}{\rho_{\rm l}(p)} = 1, \qquad m_k = \rho_k \alpha_k, \tag{6}$$

obtained from the volume fraction equation $\alpha_g + \alpha_l = 1$. More precisely, we obtain mixture mass fluxes $F_k$ of the form

$$F_{\rm l} = \kappa \left( \rho_{\rm g}\alpha_{\rm l}\frac{\partial \rho_{\rm l}}{\partial p}F_{\rm l}^{\rm D} + \rho_{\rm l}\alpha_{\rm g}\frac{\partial \rho_{\rm g}}{\partial p}F_{\rm l}^{\rm A} + \rho_{\rm l}\alpha_{\rm l}\frac{\partial \rho_{\rm l}}{\partial p}(F_{\rm g}^{\rm D} - F_{\rm g}^{\rm A}) \right)$$
$$F_{\rm g} = \kappa \left( \rho_{\rm l}\alpha_{\rm g}\frac{\partial \rho_{\rm g}}{\partial p}F_{\rm g}^{\rm D} + \rho_{\rm g}\alpha_{\rm l}\frac{\partial \rho_{\rm l}}{\partial p}F_{\rm g}^{\rm A} + \rho_{\rm g}\alpha_{\rm g}\frac{\partial \rho_{\rm g}}{\partial p}(F_{\rm l}^{\rm D} - F_{\rm l}^{\rm A}) \right),$$

where $\kappa$ is given by (5). We also verify that under natural assumptions on the $F_k^A$ flux component and the $F_k^D$ flux component, the resulting MF schemes possess certain "good" properties relevant for the approximation properties of numerical schemes in general for the two-fluid model. These results are stated in Lemma 1 and Lemma 2.

More specifically, Lemma 1 states that the MF mass fluxes recover the numerical fluxes of an exact riemann solver for a moving or stationary contact discontinuity. Lemma 2 ensures that Abrall's principle [1] is satisfied; *a flow, uniform in velocity and pressure must remain uniform during its temporal evolution.* The fact that this principle is obeyed, ensures that the use of the pressure evolution equation (4) in the discretization of the non-conservative pressure term is consistent with basic physcial understanding of two-phase flow phenomena.

Based on the semi-discrete MF scheme, we then proceed to the construction of fully discrete schemes. Motivated by previous investigations of the current two-fluid model (1) for certain hybrid FVS/FDS type of schemes, see [9, 12], we propose here to use an AUSMD/V-type discretization (originally proposed for the Euler equations in [32]) for the numerical mass flux component $F_k^A$ as well as for the discretization of the convective terms $g_k = \rho_k \alpha_k v_k^2$ of the momentum equations. In this sense the present work can be considered as an extension to a weakly implicit version of the MF-AUSMD scheme we developed in [12]. The Mixture Flux scheme studied in [12] was developed in the same framework as presented in this work, however, only pure explicit time discretizations was considered there. We emphasize that the approach presented in this paper should be general enough to apply for other flux-splitting schemes as well.

In particular, we perform numerical experiments for this weakly implicit MF-AUSMD scheme, denoted as WIMF-AUSMD, which indicate that the scheme in fact is subject to the weak CFL condition (3). More precisely, we observe:

- For a typical shock tube problem the WIMF-AUSMD scheme give non-oscillatory approximations of all waves, as opposed to the explicit AUSMD scheme investigated in [9] but similar to the explicit MF-AUSMD scheme in [12]. Comparison with a Roe scheme shows that the resolution of the volume fraction waves is very similar for both schemes whereas the resolution of sonic waves is more diffusive for the WIMF-AUSMD scheme.
- For a typical mass transport problem, like the classical water faucet problem, the strong features of the proposed WIMF-AUSMD scheme is clearly observed. Exploiting the possibility to take timesteps determined by (3), which in this case implies that the timestep is chosen to be more than 50 times larger than the timestep we use for the explicit Roe scheme, the WIMF-AUSMD scheme outperforms the Roe scheme in the resolution of the volume fraction wave.
- Numerical tests demonstrate that by employing a minor modification, similar to the one used in [9, 12], the good features of the WIMF-AUSMD scheme carries over to more difficult flow cases which locally involve transition from two-phase to single-phase flow.

Most importantly, the MF approach allows us to unify two different aspects of two-phase flow calculation; namely producing a high level of accuracy on volume fraction waves while allowing for violation of the sonic CFL criterion.

Our paper is organized as follows: In Section 2 we present the two-fluid model we will be working with. In Section 3 the MF approach is presented in a semi-discrete setting where the pressure evolution equation is introduced as well as the construction of mixture mass fluxes. These two steps constitute the main components of the Mixture Flux (MF) methods. In Section 4 we present a straightforward analysis, similar to the one presented in [12], demonstrating that the MF schemes possess some desirable properties relevant for their approximation properties.

Based on the semidiscrete scheme of Section 3, we then in Section 5, 6, and 7 proceed to construct fully discrete schemes which possess the properties identified in Section 4. In Section 8 we present numerical simulations where we attempt to shed light on the issues of stability, robustness and accuracy for the scheme. Particularly, we investigate how the scheme can handle a transition to one-phase flow using a transition fix similar to the one introduced in [9].

## 2. The Two-Fluid Model

Throughout this paper we will be concerned with the common two-fluid model formulated by stating separate conservation equations for mass and momentum for the two fluids, which we will denote as a gas (g) and a liquid (l) phase. The model is identical to the model previously considered by Evje and Flatten [9] and will be only briefly restated here. For a closer description of the terms and their significance, we refer to the previous work and the references therein.

### 2.1. Generally.

We let $\mathbf{U}$ be the vector of conserved variables

$$\mathbf{U} = \begin{bmatrix} \rho_{\mathrm{g}}\alpha_{\mathrm{g}} \\ \rho_{\mathrm{l}}\alpha_{\mathrm{l}} \\ \rho_{\mathrm{g}}\alpha_{\mathrm{g}}v_{\mathrm{g}} \\ \rho_{\mathrm{l}}\alpha_{\mathrm{l}}v_{\mathrm{l}} \end{bmatrix} = \begin{bmatrix} m_{\mathrm{g}} \\ m_{\mathrm{l}} \\ I_{\mathrm{g}} \\ I_{\mathrm{l}} \end{bmatrix}. \tag{7}$$

By using the notation $\Delta p = p - p^i$, where $p^i$ is the interfacial pressure, and $\tau_k = (p^i - p)\partial_x \alpha_k$, we see that the model (1) can be written on the form

- Conservation of mass

$$\frac{\partial}{\partial t}\left(\rho_{\mathrm{g}}\alpha_{\mathrm{g}}\right) + \frac{\partial}{\partial x}\left(\rho_{\mathrm{g}}\alpha_{\mathrm{g}}v_{\mathrm{g}}\right) = 0, \tag{8}$$

$$\frac{\partial}{\partial t}\left(\rho_{\mathrm{l}}\alpha_{\mathrm{l}}\right) + \frac{\partial}{\partial x}\left(\rho_{\mathrm{l}}\alpha_{\mathrm{l}}v_{\mathrm{l}}\right) = 0, \tag{9}$$

- Conservation of momentum

$$\frac{\partial}{\partial t}\left(\rho_{\mathrm{g}}\alpha_{\mathrm{g}}v_{\mathrm{g}}\right) + \frac{\partial}{\partial x}\left(\rho_{\mathrm{g}}\alpha_{\mathrm{g}}v_{\mathrm{g}}^2 + \alpha_{\mathrm{g}}\Delta p\right) + \alpha_{\mathrm{g}}\frac{\partial}{\partial x}(p - \Delta p) = Q_{\mathrm{g}} + M_g^D, \tag{10}$$

$$\frac{\partial}{\partial t}\left(\rho_{\mathrm{l}}\alpha_{\mathrm{l}}v_{\mathrm{l}}\right) + \frac{\partial}{\partial x}\left(\rho_{\mathrm{l}}\alpha_{\mathrm{l}}v_{\mathrm{l}}^2 + \alpha_{\mathrm{l}}\Delta p\right) + \alpha_{\mathrm{l}}\frac{\partial}{\partial x}(p - \Delta p) = Q_{\mathrm{l}} + M_l^D, \tag{11}$$

where for phase $k$ the nomenclature is as follows

| | |
|---|---|
| $\rho_k$ | - density |
| $p$ | - pressure |
| $v_k$ | - velocity |
| $\alpha_k$ | - volume fraction |
| $\Delta p$ | - pressure correction at the gas-liquid interface |
| $Q_k$ | - momentum sources (due to gravity, friction, etc) |
| $M_k^D$ | - interfacial drag force. |

The volume fractions satisfy

$$\alpha_{\mathrm{g}} + \alpha_{\mathrm{l}} = 1. \tag{12}$$

For the numerical simulations presented in this work we assume the simplified thermodynamic relations

$$\rho_{\mathrm{l}} = \rho_{\mathrm{l},0} + \frac{p - p_0}{a_{\mathrm{l}}^2} \tag{13}$$

and

$$\rho_{\mathrm{g}} = \frac{p}{a_{\mathrm{g}}^2} \tag{14}$$

where

$$p_0 = 1 \text{ bar} = 10^5 \text{ Pa}$$

$$\rho_{\mathrm{l},0} = 1000 \text{ kg/m}^3,$$

$$a_{\mathrm{g}}^2 = 10^5 (\mathrm{m/s})^2$$

and

$$a_{\mathrm{l}} = 10^3 \text{ m/s},$$

The models (13) and (14) correspond to a general stiffened gas EOS of the form

$$p = (\gamma_k - 1) a_k^2 \rho_k - \gamma_k \pi_k,$$

where $\pi_k = (a_k^2 \rho_{k,0} - p_0)/2$ where $\rho_{k,0}$ represents the material density and $p_0$ the ambient pressure. $\gamma_k$ and $\pi_k$ are constants specific for each phase. Particularly, by choosing $\gamma_{\mathrm{l}} = 2$ we recover (13) while (14) is obtained by choosing $\gamma_{\mathrm{g}} = 2$ and $\pi_{\mathrm{g}} = 0$.

Moreover, we will treat $Q_k$ as a pure source term, assuming that it does not contain any differential operators. We use the interface pressure correction

$$\Delta p = \Delta p\,(U, \delta) = \delta \frac{\alpha_{\mathrm{g}} \alpha_{\mathrm{l}} \rho_{\mathrm{g}} \rho_{\mathrm{l}}}{\rho_{\mathrm{g}} \alpha_{\mathrm{l}} + \rho_{\mathrm{l}} \alpha_{\mathrm{g}}} (v_{\mathrm{g}} - v_{\mathrm{l}})^2, \tag{15}$$

where we set $\delta = 1.2$. This choice ensures that the model is a hyperbolic system of conservation laws, see for instance [30, 5]. Another feature of this model is that it possesses an approximate mixture sound velocity $c$ given by

$$c = \sqrt{\frac{\rho_{\mathrm{l}} \alpha_{\mathrm{g}} + \rho_{\mathrm{g}} \alpha_{\mathrm{l}}}{\frac{\partial \rho_{\mathrm{g}}}{\partial p} \rho_{\mathrm{l}} \alpha_{\mathrm{g}} + \frac{\partial \rho_{\mathrm{l}}}{\partial p} \rho_{\mathrm{g}} \alpha_{\mathrm{l}}}}. \tag{16}$$

We refer to [30, 9] for more details.

Having solved for the conservative variable $\mathbf{U}$, we need to obtain the primitive variables $(\alpha_g, p, v_g, v_l)$. For the pressure variable we see that by writing the volume fraction equation (12) in terms of the conserved variables as

$$\frac{m_{\mathrm{g}}}{\rho_{\mathrm{g}}(p)} + \frac{m_{\mathrm{l}}}{\rho_{\mathrm{l}}(p)} = 1, \tag{17}$$

we obtain a relation yielding the pressure $p(m_{\mathrm{g}}, m_{\mathrm{l}})$. Using the relatively simple form of EOS given by (13) and (14) we see that the pressure $p$ is found as a positive root of a second order polynomial. For more general EOS we must solve a non-linear system of equations, for instance by using a Newton-Rapson algorithm. Moreover, the fluid velocities $v_g$ and $v_l$ are obtained directly from the relations

$$v_g = \frac{U_3}{U_1}, \qquad v_l = \frac{U_4}{U_2}.$$

**Remark 1.** *Concerning the EOS for the liquid and gas phase, we would like to emphasize that the methods we develop do not require simple linear relations as given by* (13) *and* (14). *Formally, the only point of the algorithm which is affected by using more complicated EOS is the resolution algorithm which determines the pressure from the general relation* (17).

2.2. **Some useful differential relations.** Noting that the relation (17) can be written on the form

$$m_{\rm g} = m_{\rm g}(m_{\rm l}, p) = \left(1 - \frac{m_{\rm l}}{\rho_{\rm l}(p)}\right)\rho_{\rm g}(p),$$

we see that

$$\begin{aligned} dm_{\rm g} &= (m_{\rm g})_{m_{\rm l}} dm_{\rm l} + (m_{\rm g})_p dp \\ &= -\frac{\rho_{\rm g}}{\rho_{\rm l}} dm_{\rm l} + \left(\Big[1 - \frac{m_{\rm l}}{\rho_{\rm l}}\Big](\rho_{\rm g})_p + \Big[\frac{m_{\rm l}\rho_{\rm g}}{\rho_{\rm l}^2}\Big](\rho_{\rm l})_p\right) dp. \end{aligned}$$

In other words, we have the relation

$$dp = \kappa(\rho_{\rm l} dm_{\rm g} + \rho_{\rm g} dm_{\rm l}), \tag{18}$$

where

$$\kappa = \frac{1}{\frac{\partial \rho_{\rm l}}{\partial p}\alpha_{\rm l}\rho_{\rm g} + \frac{\partial \rho_{\rm g}}{\partial p}\alpha_{\rm g}\rho_{\rm l}}. \tag{19}$$

Similarly, noting that

$$m_{\rm g} = m_{\rm g}(\alpha_{\rm l}, p) = (1 - \alpha_{\rm l})\rho_{\rm g}(p),$$

we see that

$$\begin{aligned} dm_{\rm g} &= (m_{\rm g})_{\alpha_{\rm l}} d\alpha_{\rm l} + (m_{\rm g})_p dp \\ &= -\rho_{\rm g} d\alpha_{\rm l} + (m_{\rm g})_p dp. \end{aligned}$$

Using (18), this relation can be rewritten as

$$\begin{aligned} d\alpha_{\rm l} &= \kappa\alpha_{\rm g}(\rho_{\rm g})_p dm_{\rm l} + \left(\alpha_{\rm g}\frac{\rho_{\rm l}}{\rho_{\rm g}}(\rho_{\rm g})_p\kappa - \frac{1}{\rho_{\rm g}}\right) dm_{\rm g} \\ &= \kappa\Big(\alpha_{\rm g}(\rho_{\rm g})_p dm_{\rm l} - \alpha_{\rm l}(\rho_{\rm l})_p dm_{\rm g}\Big). \end{aligned}$$

In other words, we have

$$d\alpha_{\rm l} = \kappa(-\frac{\partial \rho_{\rm l}}{\partial p}\alpha_{\rm l} dm_{\rm g} + \frac{\partial \rho_{\rm g}}{\partial p}\alpha_{\rm g} dm_{\rm l}). \tag{20}$$

By combining (18) and (20) we can write the masses $m_k$ in terms of a "pressure" and a "volume fraction" component as follows:

$$dm_{\rm g} = \alpha_{\rm g}\frac{\partial \rho_{\rm g}}{\partial p} dp - \rho_{\rm g} d\alpha_{\rm l} \tag{21}$$

and

$$dm_{\rm l} = \alpha_{\rm l}\frac{\partial \rho_{\rm l}}{\partial p} dp + \rho_{\rm l} d\alpha_{\rm l}. \tag{22}$$

The relations (18) and (20) reflect that differentials of the primitive variables $\alpha_{\rm l}$ and $p$ generally depend strongly on properties of the mixture of both masses through the differentials $dm_{\rm g}$ and $dm_{\rm l}$. Later we will derive numerical mass fluxes which are consistent with the differential relations (18)–(22).

2.3. **A pressure evolution equation.** The relation (17) gives the pressure $p = p(m_g, m_l)$ through a state relation. Now we describe another procedure for determining the pressure through a dynamic relation.

Multiplying the gas mass conservation equation with $\kappa\rho_l$ and the liquid mass conservation equation with $\kappa\rho_g$ and adding the two resulting equations, we get

$$\kappa\rho_l\frac{\partial}{\partial t}m_g + \kappa\rho_g\frac{\partial}{\partial t}m_l + \kappa\rho_l\frac{\partial}{\partial x}\left(\rho_{\rm g}\alpha_{\rm g}v_{\rm g}\right) + \kappa\rho_g\frac{\partial}{\partial x}\left(\rho_{\rm l}\alpha_{\rm l}v_{\rm l}\right) = 0.$$

In view of (18) we get the following non-conservative pressure evolution equation

$$\frac{\partial p}{\partial t} + \kappa\left(\rho_{\rm l}\frac{\partial}{\partial x}\left(\rho_{\rm g}\alpha_{\rm g}v_{\rm g}\right) + \rho_{\rm g}\frac{\partial}{\partial x}\left(\rho_{\rm l}\alpha_{\rm l}v_{\rm l}\right)\right) = 0 \tag{23}$$

where $\kappa$ is given by (19). Coupling this pressure evolution equation to the momentum equation will be an important ingredient in allowing us to break the CFL-criterion (2).

## 3. A semi-discrete scheme

In this section we construct semidiscrete approximations of solutions to (8)–(11). In the Sections 5, 6, and 7 we describe fully discrete approximations, and finally in Section 8 we explore properties of these fully discrete schemes for several well known two-phase flow problems.

### 3.1. General form.

It will be convenient to express the model (8)–(11) on the following form:

$$\begin{aligned} \partial_t m_k + \partial_x f_k &= 0, \\ \partial_t I_k + \partial_x g_k + \alpha_k \partial_x p + (\Delta p)\partial_x \alpha_k &= Q_k, \end{aligned} \tag{24}$$

where $k = g, l$ and

$$\begin{aligned} f_k &= \rho_k \alpha_k v_k \quad \text{and} \quad m_k = \rho_k \alpha_k \\ g_k &= \rho_k \alpha_k v_k^2 \quad \text{and} \quad I_k = \rho_k \alpha_k v_k. \end{aligned}$$

We assume that we have given approximations $\left(m_{k,j}^n, I_{k,j}^n\right) \approx \left(m_{k,j}(t^n), I_{k,j}(t^n)\right)$. Approximations $m_{k,j}(t)$ and $I_{k,j}(t)$ for $t \in (t^n, t^{n+1}]$ are now constructed by solving the following ODE problem:

$$\begin{aligned} \dot{m}_{k,j} + \delta_x F_{k,j} &= 0, \\ \dot{I}_{k,j} + \delta_x G_{k,j} + \alpha_{k,j}\delta_x P_j + (\Delta p)_j \delta_x \Lambda_{k,j} &= Q_{k,j}, \end{aligned} \tag{25}$$

subject to the initial conditions

$$m_{k,j}(t^n) = m_{k,j}^n, \qquad I_{k,j}(t^n) = I_{k,j}^n.$$

Here $\delta_x$ is the operator defined by

$$\delta_x w_j = \frac{w_{j+1/2} - w_{j-1/2}}{\Delta x}, \qquad \delta_x w_{j+1/2} = \frac{w_{j+1} - w_j}{\Delta x},$$

and $(\Delta p)_j(t) = (\Delta p)\left(U_j(t), \delta\right)$ is obtained from (15). Moreover, $F_{k,j+1/2}(t) = F_k(U_j(t), U_{j+1}(t))$, $G_{k,j+1/2}(t) = G_k(U_j(t), U_{j+1}(t))$, $P_{j+1/2}(t) = P(U_j(t), U_{j+1}(t))$, and $\Lambda_{k,j+1/2}(t) = \Lambda_k(U_j(t), U_{j+1}(t))$ are assumed to be numerical fluxes consistent with the corresponding physical fluxes, i.e.

$$\begin{aligned} F_k(U,U) &= f_k = \rho_k \alpha_k v_k \\ G_k(U,U) &= g_k = \rho_k \alpha_k v_k^2 \\ P(U,U) &= p \\ \Lambda_k(U,U) &= \alpha_k. \end{aligned}$$

The purpose now is to derive these numerical fluxes.

### 3.2. The numerical flux $\Lambda_{k,j+1/2}(t)$.

We first start with the numerical flux $\Lambda_{k,j+1/2}(t)$. Following the approach taken by others, see for example Paille [20] and Coquel et al [4], we discretize this term centrally. Thus we use the numerical flux

$$\Lambda_{k,j+1/2}(t) = \frac{\alpha_{k,j}(t) + \alpha_{k,j+1}(t)}{2}. \tag{26}$$

In the following we seek to discretize the remaining fluxes so that they are consistent with the underlying dynamics of the model. Essential information about the interplay between masses $m_k$ and pressure $p$ is given by the relation (17). We shall exploit this systematically when we devise numerical fluxes $F_{k,j+1/2}(t)$ and $P_{j+1/2}(t)$.

3.3. **The numerical flux $P_{j+1/2}(t)$.** We suggest to associate the numerical flux $P_{j+1/2}(t)$ with the solution of the pressure evolution equation (23) and (19) discretized at the cell interface $j+1/2$. More precisely, given the cell centered pressure $p_j^n \approx p(x_j, t^n)$ we determine $P_{j+1/2}(t)$ for $t \in (t^n, t^{n+1}]$ by solving the ODE

$$\begin{aligned} &\dot{P}_{j+1/2} + [\kappa_{j+1/2}\rho_{l,j+1/2}]\delta_x I_{g,j+1/2} + [\kappa_{j+1/2}\rho_{g,j+1/2}]\delta_x I_{l,j+1/2} = 0 \\ &P_{j+1/2}(t_+^n) = \frac{p_j^n + p_{j+1}^n}{2}, \end{aligned} \tag{27}$$

where the interface values $\kappa_{j+1/2}$ and $\rho_{k,j+1/2}$ are computed from $P_{j+1/2}(t)$ together with the arithmetic average (26) which defines $\alpha_{k,j+1/2}(t)$.

**Remark 2.** *The numerical flux $P_{j+1/2}(t) = P(U_j(t), U_{j+1}(t))$ is consistent with the physical flux. This follows easily since assuming that $U_j(t) = U_{j+1}(t) = U(t)$ for $t \in [t^n, t^{n+1}]$, implies that we shall solve the ODE*

$$\dot{P}_{j+1/2} = 0, \qquad P_{j+1/2}(t_+^n) = \frac{p_j^n + p_{j+1}^n}{2} = p(t^n),$$

*i.e. $P_{j+1/2}(t) = p(t^n) = p(t)$ for $t \in [t^n, t^{n+1}]$.*

3.4. **The numerical flux $F_{k,j+1/2}(t)$.** We first recall that from the masses $m_{k,j}(t)$, which in turn depend on the numerical mass fluxes $F_{k,j+1/2}(t)$ via the mass conservation equations of (25), we obtain the pressure $p_j(t)$ as well as the volume fraction $\alpha_{k,j}(t)$ by using the relation (17). In order to give more room for incorporating several properties which are relevant for accurate and non-oscillatory approximations of the pressure $p_j(t)$ and the volume fraction $\alpha_{k,j}(t)$, we suggest to describe the numerical massfluxes $F_k(t)$ as a combination of two different flux components $F_k^D(t)$ and $F_k^A(t)$ respectively.

More precisely, we associate the mass flux component $F_k^D$ with the pressure calculation $p = p(m_g, m_l)$ via the relation (17) while the $F_k^A$ component is associated with the volume fraction calculation $\alpha_k = m_k/\rho_k(p(m_g, m_l))$. An important point here is to give an appropriate description of the balance between the two components $F_k^D$ and $F_k^A$ as well as to develop the $F_k^D$- and $F_k^A$-components themselves. The first point is discussed in the following while the latter is postponed until Section 6 and 7 respectively.

From (21) and (22) we see that the mass differentials $dm_k$ can be split in a pressure component $dp$ and a volume fraction component $d\alpha$. We now want to design numerical fluxes which are consistent with this splitting, i.e. we introduce a flux component $F_p$ and $F_\alpha$ such that the mass fluxes $F_\mathrm{l}$ and $F_\mathrm{g}$ are given by

$$F_\mathrm{l} = \alpha_\mathrm{l}\frac{\partial \rho_\mathrm{l}}{\partial p}F_p + \rho_\mathrm{l}F_\alpha \tag{28}$$

and

$$F_\mathrm{g} = \alpha_\mathrm{g}\frac{\partial \rho_\mathrm{g}}{\partial p}F_p - \rho_\mathrm{g}F_\alpha. \tag{29}$$

The flux component $F_p$ is associated with the pressure, hence it is natural to assign a diffusive mass flux $F^\mathrm{D}$ for stable approximation of pressure for the various waves. Inspired by the differential relation (18) we propose to give $F_p$ the following form

$$F_p = \kappa\rho_\mathrm{g}F_\mathrm{l}^\mathrm{D} + \kappa\rho_\mathrm{l}F_\mathrm{g}^\mathrm{D} \tag{30}$$

Similarly, the flux component $F_\alpha$ is associated with the volume fraction. Hence we seek to assign an mass flux $F^\mathrm{A}$ such that an accurate resolution of the volume fraction variable can be obtained. Inspired by the differential relation (20), we propose to give $F_\alpha$ the following form

$$F_\alpha = \kappa\frac{\partial \rho_\mathrm{g}}{\partial p}\alpha_\mathrm{g}F_\mathrm{l}^\mathrm{A} - \kappa\frac{\partial \rho_\mathrm{l}}{\partial p}\alpha_\mathrm{l}F_\mathrm{g}^\mathrm{A}. \tag{31}$$

Here we note that a subscript $j+1/2$ is assumed on the fluxes and coefficients. Substituting (30) and (31) into (29) and (28) we obtain the final hybrid mass fluxes

$$F_\mathrm{l} = \kappa\left(\rho_\mathrm{g}\alpha_\mathrm{l}\frac{\partial \rho_\mathrm{l}}{\partial p}F_\mathrm{l}^\mathrm{D} + \rho_\mathrm{l}\alpha_\mathrm{g}\frac{\partial \rho_\mathrm{g}}{\partial p}F_\mathrm{l}^\mathrm{A} + \rho_\mathrm{l}\alpha_\mathrm{l}\frac{\partial \rho_\mathrm{l}}{\partial p}(F_\mathrm{g}^\mathrm{D} - F_\mathrm{g}^\mathrm{A})\right) \tag{32}$$

and

$$F_{\rm g} = \kappa \left( \rho_{\rm l}\alpha_{\rm g}\frac{\partial \rho_{\rm g}}{\partial p}F_{\rm g}^{\rm D} + \rho_{\rm g}\alpha_{\rm l}\frac{\partial \rho_{\rm l}}{\partial p}F_{\rm g}^{\rm A} + \rho_{\rm g}\alpha_{\rm g}\frac{\partial \rho_{\rm g}}{\partial p}(F_{\rm l}^{\rm D} - F_{\rm l}^{\rm A}) \right). \tag{33}$$

The coefficient variables at $j+1/2$ remain to be determined. We suggest finding these from the cell interface pressure $P_{j+1/2}(t)$ as well as the relation

$$\alpha_{j+1/2}(t) = \frac{1}{2}(\alpha_j(t) + \alpha_{j+1}(t))$$

which is consistent with the treatment of the coefficients of the pressure evolution equation (27).

**Remark 3.** *We remark that the consistency criterion*

$$F_k(U,U) = f_k(U) = \rho_k\alpha_k v_k,$$

*relating the physical flux $f_k$ to the numerical flux $F_k$, is satisfied for the hybrid fluxes (32) and (33) provided the fluxes $F_k^A$ and $F_k^D$ are consistent. In particular if $F_k^A = F_k^D$ the expressions (32) and (33) reduce to the trivial identity*

$$F_k = F_k^A = F_k^D.$$

3.5. **The numerical flux $G_{k,j+1/2}(t)$.** Based on the belief that the difficult and critical part is to obtain a numerical mass flux $F_{k,j+1/2}(t)$ which is consistent with the discretization of the pressure term of the momentum equations, we seek a more straightforward construction of $G_{k,j+1/2}(t)$. In particular, we want to couple this convective flux to the mass flux $F_k^A$. In order to emphasize this we use the superscript "A", i.e.

$$G_{k,j+1/2}(t) = G^A_{k,j+1/2}(t). \tag{34}$$

More precisely, we choose $G^A_{k,j+1/2}(t)$ to be consistent with the flux component $F^A_{k,j+1/2}(t)$ in the following sense: For a flow with velocities which are constant in space for the time interval $[t^n, t^{n+1}]$, that is,

$$v_{k,j}(t) = v_{k,j+1}(t) = v_k(t), \qquad t \in [t^n, t^{n+1}], \tag{35}$$

we assume that $G^A_{k,j+1/2}(t)$ takes the form

$$G^A_{k,j+1/2}(t) = v_k(t)F^A_{k,j+1/2}(t), \tag{36}$$

where $F^A_{k,j+1/2}(t)$ is the numerical flux component introduced above and assumed to be consistent with the physical flux $f_k = \rho_k\alpha_k v_k$.

**Remark 4.** *We remark that the consistency criterion*

$$G_k(U,U) = g_k(U) = \rho_k\alpha_k v_k^2,$$

*relating the numerical flux $G_k$ to the physical flux $g_k$, is satisfied for $G_k$ as given by* (36) *provided the numerical flux $F_k^A$ is consistent with the physical flux $f_k$.*

## 4. Further Development of the Mass Flux $F_{k,j+1/2}(t)$

A main issue in the resolution of two-phase flow as described by the current model is to obtain an accurate resolution of mass fronts, i.e. slow-moving volume fraction waves. Hence, in the following we want to ensure that the mass fluxes $F_k^D(t)$ and $F_k^A(t)$ are constructed so that certain "good" properties in this respect are ensured for the resulting mass flux $F_k(t)$. Particularly, we shall identify a simple characterization of some properties which $F_k^D$ and $F_k^A$ should possess.

In order to identify this characterization, we consider the contact discontinuity given by

$$\begin{gathered} p_{\rm L} = p_{\rm R} = p \\ \alpha_{\rm L} \neq \alpha_{\rm R} \\ (v_{\rm g})_{\rm L} = (v_{\rm l})_{\rm L} = (v_{\rm g})_{\rm R} = (v_{\rm l})_{\rm R} = v, \end{gathered} \tag{37}$$

for the time period $[t^n, t^{n+1}]$. All pressure terms vanish from the model (8)-(11), and it is seen that the solution to this initial value problem is simply that the discontinuity will propagate with the velocity $v$. The exact solution of the Riemann problem will then give the numerical mass flux

$$(\rho\alpha v)_{j+1/2} = \frac{1}{2}\rho(\alpha_{\rm L} + \alpha_{\rm R})v - \frac{1}{2}\rho(\alpha_{\rm R} - \alpha_{\rm L})|v|. \tag{38}$$

**Definition 1.** *A numerical flux $F$ that satisfy (38) for the contact discontinuity (37) will in the following be termed a "mass coherent" flux.*

4.1. **A "mass coherent" flux $F_k^A$.** The purpose of the flux component $F_k^A$ is to ensure accuracy at volume fraction waves. A natural requirement for $F_k^A$ is then that it should be mass coherent in the sense of Definition 1. We shall return to a more detailed specification in Section 7 but at this stage it might be instructive to briefly mention two examples of numerical mass fluxes studied before for the two fluid model [9], one which is mass coherent and one which is not mass coherent.

**Two examples.** In [9] we studied a FVS type of scheme for the current two-phase model whose mass fluxes are given by

$$(\rho\alpha v)_{j+1/2} = (\rho\alpha)_{\rm L} V^+(v_{\rm L}, c_{j+1/2}) + (\rho\alpha)_{\rm R} V^-(v_{\rm R}, c_{j+1/2}) \tag{39}$$

for each phase where $c_{j+1/2} = \max(c_L, c_R)$ and $V^\pm$ are given by

$$V^\pm(v,c) = \begin{cases} \pm\frac{1}{4c}(v \pm c)^2 & \text{if } |v| \le c \\ \frac{1}{2}(v \pm |v|) & \text{otherwise.} \end{cases}$$

Here the parameter $c$ controls the amount of numerical diffusion, and is normally associated with the physical sound velocity for the system. This flux is *not* mass coherent according to Definition 1 and leads to poor resolution of mass fronts, as was clearly observed in [9].

In [9] we also studied a modification of the mass fluxes (39) obtained by replacing $V^\pm$ by

$$\tilde{V}^\pm(v,c,\chi) = \begin{cases} \chi V^\pm(v,c) + (1-\chi)\frac{v\pm|v|}{2} & |v| < c \\ \frac{1}{2}(v \pm |v|) & \text{otherwise} \end{cases}$$

where $\chi_{\rm L}$ and $\chi_{\rm R}$ satisfy the relation

$$\chi_{\rm R}\alpha_{\rm R} - \chi_{\rm L}\alpha_{\rm L} = 0. \tag{40}$$

It is easy to verify that the resulting mass flux is mass coherent in the sense of Definition 1, and we observed in [9] that the level of accuracy was similar to that of a Roe scheme in the resolution of mass fronts.

Knowing that the total flux component $F_k$ given by (32) and (33) also should be accurate at volume fraction waves, i.e. mass coherent, we way ask: What is a minimal condition satisfied by the $F_k^D$-component which ensures that $F_k$ still becomes mass coherent?

4.2. **A "pressure coherent" flux $F_k^D$.** We note that the pressure will remain constant and uniform as the discontinuity (37) is propagating. Consequently, a natural requirement on a "good" flux $F_k^{\rm D}$ for stable pressure resolution is that it preserves the constancy of pressure for the moving or stationary contact discontinuity given by (37).

We write (18) as

$$dp = \kappa d\mu$$

where

$$d\mu = \rho_{\rm g} dm_{\rm l} + \rho_{\rm l} dm_{\rm g}. \tag{41}$$

To maintain a constant pressure we must have $d\mu = 0$. Assuming constant pressure, (41) can be integrated to yield

$$\mu = \rho_{\rm g} m_{\rm l} + \rho_{\rm l} m_{\rm g} = \rho_{\rm g}\rho_{\rm l}(\alpha_{\rm l} + \alpha_{\rm g}) = \rho_{\rm g}\rho_{\rm l}.$$

To maintain constancy of $\mu$, and hence $p$, we now insist that the flux $F_k^{\rm D}$ is a consistent numerical flux when applied to the mix mass $\mu$. That is, we impose

$$\rho_{\rm g} F^{\rm D}_{{\rm l},j+1/2} + \rho_{\rm l} F^{\rm D}_{{\rm g},j+1/2} = \rho_{\rm g}\rho_{\rm l} v. \tag{42}$$

for the contact discontinuity (37).

**Definition 2.** *A pair of numerical fluxes $(F_l, F_g)$ that satisfy (42) for the contact discontinuity (37) will in the following be termed "pressure coherent" fluxes.*

In particular, we note that the FVS mass fluxes (39) as well as the upwind fluxes (38) are pressure coherent. Thus, the class of *mass coherent* fluxes is contained in the class of *pressure coherent* fluxes. However, it should be noted that we can easily construct a pair of perfectly valid mass fluxes, in the sense that they are consistent with the physical flux, that are *not* pressure coherent. Consider for example the stationary contact discontinuity (37) with $v = 0$. Let $F_{\mathrm{g}}$ be given by the upwind flux (38) and $F_{\mathrm{l}}$ be given by the FVS flux (39). Then

$$\rho_{\mathrm{g}} F_{\mathrm{l},j+1/2} + \rho_{\mathrm{l}} F_{\mathrm{g},j+1/2} = \rho_{\mathrm{g}}\rho_{\mathrm{l}} \frac{c}{4} \left( (\alpha_{\mathrm{l}})_{\mathrm{L}} - (\alpha_{\mathrm{l}})_{\mathrm{R}} \right) \neq 0,$$

defying the requirement (42). Thus, this mass flux is neither pressure nor mass coherent in the sense of Definition 1 and 2.

4.3. **Construction of mass coherent fluxes $F_k(t)$.** We now state the following important lemma:

**Lemma 1.** *Let the mixture fluxes (32) and (33) be constructed from pressure coherent fluxes $F_k^D$ in the sense of Definition 2, and mass coherent fluxes $F_k^A$ in the sense of Definition 1. Then the hybrid fluxes (32) and (33) reduce to the upwind fluxes (38) on the contact discontinuity (37), i.e. they are mass coherent.*

*Proof.* We consider the hybrid liquid mass flux (32) and assume that $v \geq 0$. Remembering that a subscript $j + 1/2$ is assumed on the variables, we write the flux as

$$F_{\mathrm{l}} = \kappa \left( \alpha_{\mathrm{l}} \frac{\partial \rho_{\mathrm{l}}}{\partial p} (\rho_{\mathrm{g}} F_{\mathrm{l}}^{\mathrm{D}} + \rho_{\mathrm{l}} F_{\mathrm{g}}^{\mathrm{D}}) + \rho_{\mathrm{l}} \alpha_{\mathrm{g}} \frac{\partial \rho_{\mathrm{g}}}{\partial p} F_{\mathrm{l}}^{\mathrm{A}} - \rho_{\mathrm{l}} \alpha_{\mathrm{l}} \frac{\partial \rho_{\mathrm{l}}}{\partial p} F_{\mathrm{g}}^{\mathrm{A}} \right) \tag{43}$$

Using the required properties of $F_k^{\mathrm{A}}$ and $F_k^{\mathrm{D}}$ given by Definition 1 and Definition 2 respectively, we obtain

$$F_{\mathrm{l}} = \kappa \left( \alpha_{\mathrm{l}} \frac{\partial \rho_{\mathrm{l}}}{\partial p} \rho_{\mathrm{g}} \rho_{\mathrm{l}} v + \rho_{\mathrm{l}}^2 \alpha_{\mathrm{g}} \frac{\partial \rho_{\mathrm{g}}}{\partial p} (\alpha_{\mathrm{l}})_{\mathrm{L}} v - \rho_{\mathrm{g}} \rho_{\mathrm{l}} \alpha_{\mathrm{l}} \frac{\partial \rho_{\mathrm{l}}}{\partial p} (1 - (\alpha_{\mathrm{l}})_{\mathrm{L}}) v \right) = \rho_{\mathrm{l}} (\alpha_{\mathrm{l}})_{\mathrm{L}} v, \tag{44}$$

where we have used that

$$\rho_{j+1/2} = \rho_L = \rho_R \tag{45}$$

which follows from the assumption of constant, uniform pressure. Spatial and phasic symmetry directly give the corresponding results for $F_{\mathrm{g}}$ and $v \leq 0$, completing the proof. □

**Remark 5.** *The importance of Lemma 1 lies in the fact that it allows us to search for an appropriate flux component $F_k^D$* **outside** *the class of mass coherent fluxes, and still, as long as $F_k^D$ is pressure coherent and $F_k^A$ is mass coherent, we obtain mass coherent fluxes $F_k$. This is the crucial mechanism of the decomposition* (32) *and* (33)*.*

4.4. **The class of Mixture Flux (MF) methods.** Motivated by the mixture mass fluxes (32) and (33) as well as the use of the pressure evolution equation (27), we propose the following definition:

**Definition 3.** *We will use the term* **Mixture Flux** *(MF) methods to denote numerical algorithms which are constructed within the above semi-discrete framework, that is: (i) the numerical mass flux $F_{k,j+1/2}(t)$ is given by the mixture fluxes (32) and (33) where $F_k^D$ is pressure coherent in the sense of Definition 2 and $F_k^A$ is mass coherent in the sense of Definition 1: (ii) the numerical pressure flux $P_{j+1/2}(t)$ is obtained as the solution of* (27)*; (iii) the convective flux $G^A_{k,j+1/2}(t)$ satisfies* (36) *for flow with uniform velocity* (35)*.*

Next, we apply Lemma 1 to verify that the MF methods satisfy the following principle due to Abgrall [1, 24, 25]:
*A flow, uniform in pressure and velocity must remain uniform in the same variables during its time evolution.*

**Lemma 2.** *The MF methods given by Definition 3, obey Abgrall's principle.*

*Proof.* We assume that we have the contact discontinuity given by (37) and that it remains unchanged during the time interval $[t^n, t^{n+1}]$. In view of Lemma 1 and the fact that the convective fluxes $G^{\mathrm{A}}_{k,j+1/2}(t)$ of the momentum equations of the MF methods satisfy (36), we immediately conclude that the semidiscrete model (25) takes the form

$$\begin{aligned} \dot{m}_{k,j} + \delta_x(\rho_k \alpha_k v_k)_j &= 0, \\ v\,\dot{m}_{k,j} + v\delta_x(\rho_k \alpha_k v_k)_j + \alpha_{k,j}\delta_x P_j + (\Delta p)_j \delta_x \Lambda_{k,j} &= 0, \end{aligned} \tag{46}$$

where $(\rho_k \alpha_k v_k)_{j+1/2}$ is on the form (38). In view of (15) we conclude that $(\Delta p)_j = 0$. Moreover, we see that (27) reduces to

$$\begin{aligned} \dot{P}_{j+1/2} &= -[\kappa_{j+1/2}\rho_{l,j+1/2}]\delta_x I_{g,j+1/2} + [\kappa_{j+1/2}\rho_{g,j+1/2}]\delta_x I_{l,j+1/2} \\ &= -\kappa_{j+1/2}[\rho_l \rho_g v \delta_x \alpha_{g,j+1/2} + \rho_g \rho_l v \delta_x \alpha_{l,j+1/2}] = 0, \end{aligned}$$

since $\alpha_{\mathrm{g}} + \alpha_{\mathrm{l}} = 1$. In other words,

$$P_{j+1/2}(t) = P_{j+1/2}(t^n_+) = \frac{p^n_j + p^n_{j+1}}{2} = p, \qquad t \in (t^n, t^{n+1}],$$

for all $j$. Consequently, $\delta_x P_j = 0$, and we can conclude that Abgrall's principle holds for the MF methods. □

**Remark 6.** *We may consider the class of schemes introduced in this paper, which all employ mass fluxes of the form (32) and (33), as genuine* **two-phase** *flux splitting schemes. This flux splitting is based on a decomposition of the mass fluxes into several phasic components, i.e. one specific mass flux involves components from both the liquid and gas phase. In this sense the class of schemes we study is fundamentally different from the solution method used in e.g.* [4, 19, 20, 9] *where the underlying philosophy is to solve the two-phase model basically as two single-phase problems.*

In the next sections (Section 5,6 and 7) we shall specify fully discrete schemes based on the semi-discrete scheme presented in Section 3 and 4. In particular, we will develop a flux component $F^D_k$ which is pressure coherent, but not mass coherent. This flux component is constructed so that it allows us to obtain a stable pressure $p = p(m_g, m_l)$ via (17), even for time-steps which obey only the weak CFL condition (2). The fact that it is pressure coherent, i.e. satisfies (42) for a contact discontinuity (37), ensures that it does not introduce undesirable numerical dissipation at volume fraction waves. For the construction of appropriate flux components $F^{\mathrm{A}}_k$ and $G^{\mathrm{A}}_k$ we are going to use the AUSMV/D framework developed by Wada and Liou [32] for Euler equations and adapted to the two-phase flow model in [9], see also [20] for similar type of schemes for the two-fluid model.

## 5. Fully Discrete Numerical Schemes

We now consider a fully discrete scheme corresponding to the semi-discrete scheme given by (25), (26), (27), (32), (33), and (34).

**General form.**

- Gas Mass

$$\frac{m^{n+1}_{g,j} - m^n_{g,j}}{\Delta t} = -\delta_x F^{n+1/2}_{g,j} \tag{47}$$

- Liquid Mass

$$\frac{m^{n+1}_{l,j} - m^n_{l,j}}{\Delta t} = -\delta_x F^{n+1/2}_{l,j} \tag{48}$$

- Pressure at cell interface

$$\begin{aligned} &\frac{P^{n+1}_{j+1/2} - \frac{1}{2}(p^n_j + p^n_{j+1})}{\Delta t} \\ &= -(\kappa\rho_{\mathrm{l}})^n_{j+1/2}\frac{I^{n+1}_{g,j+1} - I^{n+1}_{g,j}}{\Delta x} - (\kappa\rho_{\mathrm{g}})^n_{j+1/2}\frac{I^{n+1}_{l,j+1} - I^{n+1}_{l,j}}{\Delta x} \end{aligned} \tag{49}$$

- Gas Momentum

$$\begin{aligned}&\frac{I_{g,j}^{n+1}-I_{g,j}^{n}}{\Delta t}\\&=-\delta_x(G^A)_{g,j}^n-\alpha_{g,j}^n\frac{P_{j+1/2}^{n+1}-P_{j-1/2}^{n+1}}{\Delta x}-(\Delta p)_j^n\delta_x\Lambda_{g,j}^n+(Q_{\mathrm{g}})_j^n.\end{aligned}\tag{50}$$

- Liquid Momentum

$$\begin{aligned}&\frac{I_{l,j}^{n+1}-I_{l,j}^{n}}{\Delta t}\\&=-\delta_x(G^A)_{l,j}^n-\alpha_{l,j}^n\frac{P_{j+1/2}^{n+1}-P_{j-1/2}^{n+1}}{\Delta x}-(\Delta p)_j^n\delta_x\Lambda_{l,j}^n+(Q_{\mathrm{l}})_j^n.\end{aligned}\tag{51}$$

Here we have introduced the shorthands

$$m_k=\rho_k\alpha_k,\qquad I_k=m_kv_k.$$

In accordance with (26) we use

$$\Lambda_{k,j+1/2}^n=\frac{\alpha_{k,j}^n+\alpha_{k,j+1}^n}{2}\tag{52}$$

and where $(\Delta p)_j^n=(\Delta p)\left(U_j^n,\delta\right)$ is evaluated from (15). For the discretization of the pressure evolution equation (27) as given by (49), we keep the coefficients $\kappa\rho_k$ fixed at timelevel $t^n$ whereas the massfluxes $I_k$ are given an implicit treatment as they are discretized at timelevel $t^{n+1}$. Particularly, this enforces a coupling between the equations (49), (50), and (51). We end up with solving a linear system $Ax=b$ where $A$ is a sparse banded matrix with 2 superdiagonals and 2 subdiagonals.

For the numerical mass fluxes $F_{k,j+1/2}^{n+1/2}$ the purpose of the "$n+1/2$" notation is to indicate that we shall discretize some terms at time level $t^n$, others at time $t^{n+1}$. More precisely, we propose to use the following time discretization for the mass fluxes (32) and (33) (for simplicity we have again dropped the subscript $j+1/2$):

$$F_{\mathrm{l}}^{n+1/2}=[\kappa\rho_{\mathrm{g}}\alpha_{\mathrm{l}}(\rho_{\mathrm{l}})_p]^n(F_{\mathrm{l}}^{\mathrm{D}})^{n+1/2}+[\kappa\rho_{\mathrm{l}}\alpha_{\mathrm{g}}(\rho_{\mathrm{g}})_p]^n(F_{\mathrm{l}}^{\mathrm{A}})^n+[\kappa\rho_{\mathrm{l}}\alpha_{\mathrm{l}}(\rho_{\mathrm{l}})_p]^n\Big((F_{\mathrm{g}}^{\mathrm{D}})^{n+1/2}-(F_{\mathrm{g}}^{\mathrm{A}})^n\Big)\tag{53}$$

and

$$F_{\mathrm{g}}^{n+1/2}=[\kappa\rho_{\mathrm{l}}\alpha_{\mathrm{g}}(\rho_{\mathrm{g}})_p]^n(F_{\mathrm{g}}^{\mathrm{D}})^{n+1/2}+[\kappa\rho_{\mathrm{g}}\alpha_{\mathrm{l}}(\rho_{\mathrm{l}})_p]^n(F_{\mathrm{g}}^{\mathrm{A}})^n+[\kappa\rho_{\mathrm{g}}\alpha_{\mathrm{g}}(\rho_{\mathrm{g}})_p]^n\Big((F_{\mathrm{l}}^{\mathrm{D}})^{n+1/2}-(F_{\mathrm{l}}^{\mathrm{A}})^n\Big).\tag{54}$$

In other words, the flux component $F_k^A$ is kept at the timelevel $t^n$ whereas the flux component $F_k^D$ involves terms at timelevel $t^{n+1}$. Particularly, we want to make use of the updated momentums $I_k^{n+1}$ obtained from solving (49)–(51) in the expressions for $F_k^D$. We describe the details in the next section.

It turns out that this implicit treatment is crucial in order to maintain the stability of the scheme for large time steps. This aspect is explored in more detail in Section 8.1. Note that we shall not need to solve any linear system here as will become clear from Section 6. In view of (53) and (54), we see that what remains, is to specify the numerical flux components $(F_k^A)_{j+1/2}^n$ and $(G_k^A)_{j+1/2}^n$, as well as $(F_k^D)_{j+1/2}^{n+1/2}$. We start with the latter.

**Remark 7.** *The discretization of the pressure equation at the cell interface can be viewed as a staggered Lax-Friedrichs scheme. We assume that the pressure $p_j$ is found from the masses $m_j$ by (17). The interdependence between $P_{j+1/2}$ and the couple $(p_j,p_{j+1})$ through the proposed discretization* (49) *ensures that the numerical flux $P_{j+1/2}$ is consistent with the physical flux, as pointed out in Remark 2.*

## 6. Specification of the pressure coherent convective flux $(F_k^D)^{n+1/2}$

Due to the fact that the mass flux component $F_k^D$ is associated with the pressure calculation as described in Section 3.4, it is natural to choose a discretization of this flux which is consistent with the discretization of the pressure evolution equation. On the semi-discrete level, in view of (27), we therefore propose to consider the following discretization of the mass conservation equations

$$\begin{aligned} \dot{m}_{k,j+1/2} + \delta_x I_{k,j+1/2} &= 0, \qquad t \in (t^n, t^{n+1}] \\ m_{k,j+1/2}(t_+^n) &= \frac{m_{k,j}^n + m_{k,j+1}^n}{2}. \end{aligned} \tag{55}$$

We now suggest to average as follows:

$$m_{k,j}(t) = \frac{1}{2}\left(m_{k,j-1/2}(t) + m_{k,j+1/2}(t)\right),$$

which implies that

$$\dot{m}_{k,j}\,(t) = \frac{1}{2}\left(\dot{m}_{k,j-1/2}\,(t) + \dot{m}_{k,j+1/2}\,(t)\right). \tag{56}$$

By substituting (55) into (56) we obtain the following ODE equation for $m_{k,j}(t)$:

$$\begin{aligned} \dot{m}_{k,j} + \frac{1}{2\Delta x}(I_{k,j+1} - I_{k,j-1}) &= 0, \qquad t \in (t^n, t^{n+1}] \\ m_{k,j}(t_+^n) &= \frac{1}{4}\Big(m_{k,j-1}^n + 2m_{k,j}^n + m_{k,j+1}^n\Big). \end{aligned} \tag{57}$$

To achieve conservative mass treatment while maintaining CFL-stability, it is clear that we somehow should take advantage of the already implicitly calculated mass fluxes $I_{k,j}^{n+1}$ obtained from solving (49)–(51). A fully discrete version of (57) which employs this updated mass fluxes $I_{k,j}^{n+1}$ is then given by

$$\frac{m_{k,j}^{n+1} - \frac{1}{4}\left(2m_{k,j}^n + m_{k,j-1}^n + m_{k,j+1}^n\right)}{\Delta t} + \frac{1}{2\Delta x}\left(I_{k,j+1}^{n+1} - I_{k,j-1}^{n+1}\right) = 0, \tag{58}$$

which can be written on flux-conservative form (47) and (48) with the numerical fluxes

$$(F_k^D)_{j+1/2}^{n+1/2} = \frac{1}{2}(I_{k,j}^{n+1} + I_{k,j+1}^{n+1}) + \frac{1}{4}\frac{\Delta x}{\Delta t}(m_{k,j}^n - m_{k,j+1}^n). \tag{59}$$

Now we may solve for the masses $m_{k,j}^{n+1}$ using the fluxes (59), taking advantage of the fact that they emerge through an implicit coupling to the pressure. We found that by doing this we were able to violate the CFL-criterion for sonic waves. This is explored in more detail in the numerical Section 8.1.

Next, we check that the proposed flux $F_k^D$ possesses the "pressure coherent" property of Definition 2.

**Proposition 1.** *The flux component $F_k^D$ given by (59) is pressure coherent in the sense of Definition 2.*

*Proof.* We just need to check that $F_k^D$ satisfies the relation (42). Using the constants of (37), a direct calculation gives

$$\begin{aligned} \rho_{\mathrm{g}}(F_{\mathrm{l}}^D)_{j+1/2}^{n+1/2} + \rho_{\mathrm{l}}(F_{\mathrm{g}}^D)_{j+1/2}^{n+1/2} &= \rho_{\mathrm{g}}\rho_{\mathrm{l}}\left[\frac{v}{2}(\alpha_{\mathrm{l},j}^{n+1} + \alpha_{\mathrm{l},j+1}^{n+1}) + \frac{\Delta x}{4\Delta t}(\alpha_{\mathrm{l},j}^n - \alpha_{\mathrm{l},j+1}^n)\right] \\ &\quad + \rho_{\mathrm{g}}\rho_{\mathrm{l}}\left[\frac{v}{2}(\alpha_{\mathrm{g},j}^{n+1} + \alpha_{\mathrm{g},j+1}^{n+1}) + \frac{\Delta x}{4\Delta t}(\alpha_{\mathrm{g},j}^n - \alpha_{\mathrm{g},j+1}^n)\right] \\ &= \rho_{\mathrm{g}}\rho_{\mathrm{l}}\left[\frac{v}{2}(1+1) + \frac{\Delta x}{4\Delta t}(1-1)\right] = \rho_{\mathrm{g}}\rho_{\mathrm{l}} v. \end{aligned}$$

□

Note however, by direct calculation, that this $F_k^{\mathrm{D}}$ mass flux component is *not* mass coherent in the sense of Definition 1.

**Remark 8.** *Our experience is that it is essential to use a discretization of the mass equations, represented by the $F_k^D$ flux component* (59)*, which is consistent with the one used for the pressure evolution equation in order to obtain non-oscillatory (stable) approximations for the pressure when large time steps governed by* (2) *are employed. However, this leads to mass fluxes $F_k^D$ which are not mass coherent according to Definition 1.*

*Consequently, by using $F_k^D$ only as mass fluxes, i.e. $F_k = F_k^D$, we must expect that a strong smearing of volume fraction waves is introduced. However, Lemma 1 states that by the introduction of the mixture mass fluxes* (32) *and* (33) *we only need $F_k^D$ to satisfy the weaker "pressure coherent"-condition given by Definition 2, and still we retain mass fluxes $F_k$ which are mass coherent as long as we use a "mass coherent" $F_k^A$ component.*

## 7. Specification of the mass coherent convective fluxes $(F_k^A)^n$ and corresponding convective momentum fluxes $(G_k^A)^n$

In this section we look for appropriate choices for the numerical flux components $F_k^A$ and $G_k^A$ by considering so-called hybrid FDS/FVS type of schemes. Such schemes have been explored for the present two-fluid model more recently [9, 12]. We here briefly restate the numerical convective fluxes $(\rho\alpha v)_{j+1/2}$ and $(\rho\alpha v^2)_{j+1/2}$ corresponding to the flux splitting schemes we investigated in [9].

### 7.1. FVS/van Leer.

We consider the velocity splitting formulas used in previous works [15, 32, 7, 8, 9].

$$V^{\pm}(v,c) = \begin{cases} \pm\frac{1}{4c}(v \pm c)^2 & \text{if } |v| \le c \\ \frac{1}{2}(v \pm |v|) & \text{otherwise.} \end{cases} \tag{60}$$

Here the parameter $c$ controls the amount of numerical diffusion, and is normally associated with the physical sound velocity for the system. Following [9] we here assume that the sound velocity is given by (16). Following the standard set by earlier works [32, 7, 9] we choose a common sound velocity

$$c_{j+1/2} = \max(c_{\mathrm{L}}, c_{\mathrm{R}})$$

at the cell interface.

(1) *Mass Flux.* We let the numerical mass flux $(\rho\alpha v)_{j+1/2}$ for FVS and van Leer be given as

$$(\rho\alpha v)_{j+1/2} = (\rho\alpha)_{\mathrm{L}} V^+(v_{\mathrm{L}}, c_{j+1/2}) + (\rho\alpha)_{\mathrm{R}} V^-(v_{\mathrm{R}}, c_{j+1/2}) \tag{61}$$

for each phase.

(2) *Momentum Flux.* We let the numerical convective momentum flux $(\rho\alpha v^2)_{j+1/2}$ be given as

- FVS:

$$(\rho\alpha v^2)_{j+1/2} = V^+(v_{\mathrm{L}}, c_{j+1/2})(\rho\alpha v)_{\mathrm{L}} + V^-(v_{\mathrm{R}}, c_{j+1/2})(\rho\alpha v)_{\mathrm{R}} \tag{62}$$

- van Leer:

$$(\rho\alpha v^2)_{j+1/2} = \frac{1}{2}(\rho\alpha v)_{j+1/2}(v_{\mathrm{L}} + v_{\mathrm{R}}) - \frac{1}{2}|(\rho\alpha v)_{j+1/2}|(v_{\mathrm{R}} - v_{\mathrm{L}}) \tag{63}$$

### 7.2. AUSMV/AUSMD.

Following [9], we consider the convective fluxes associated with the AUSMV and AUSMD scheme obtained by replacing the splitting formulas $V^{\pm}$ used in (61)–(63) with the less diffusive pair

$$\tilde{V}^{\pm}(v,c,\chi) = \begin{cases} \chi V^{\pm}(v,c) + (1-\chi)\frac{v \pm |v|}{2} & |v| < c \\ \frac{1}{2}(v \pm |v|) & \text{otherwise} \end{cases} \tag{64}$$

where

$$\chi_{\mathrm{L}} = \frac{2(\rho/\alpha)_{\mathrm{L}}}{(\rho/\alpha)_{\mathrm{L}} + (\rho/\alpha)_{\mathrm{R}}} \tag{65}$$

and

$$\chi_{\mathrm{R}} = \frac{2(\rho/\alpha)_{\mathrm{R}}}{(\rho/\alpha)_{\mathrm{L}} + (\rho/\alpha)_{\mathrm{R}}} \tag{66}$$

for each phase.

**Definition 4.** *Using the terminology of Wada and Liou* [32]*, we will henceforth refer to the FVS scheme modified with the splittings* (64) *and the choice of* $\chi$ *described by* (65) *and* (66) *as the* **AUSMV** *scheme. That is, the convective fluxes of AUSMV are described by*

- Mass Flux:
$$(\rho\alpha v)^{\text{AUSMV}}_{j+1/2} = (\rho\alpha)_L \tilde{V}^+(v_L, c_{j+1/2}, \chi_L) + (\rho\alpha)_R \tilde{V}^-(v_R, c_{j+1/2}, \chi_R) \tag{67}$$
- Momentum Flux:
$$(\rho\alpha v^2)^{\text{AUSMV}}_{j+1/2} = \tilde{V}^+(v_L, c_{j+1/2}, \chi_L)(\rho\alpha v)_L + \tilde{V}^-(v_R, c_{j+1/2}, \chi_R)(\rho\alpha v)_R. \tag{68}$$

**Definition 5.** *Similarly, we will henceforth refer to the van Leer scheme modified with the splittings* (64) *and the choice of* $\chi$ *described by* (65) *and* (66) *as the* **AUSMD** *scheme. That is, the convective fluxes of AUSMD are described by*

- Mass Flux:
$$(\rho\alpha v)^{\text{AUSMD}}_{j+1/2} = (\rho\alpha)_L \tilde{V}^+(v_L, c_{j+1/2}, \chi_L) + (\rho\alpha)_R \tilde{V}^-(v_R, c_{j+1/2}, \chi_R) \tag{69}$$
- Momentum Flux:
$$(\rho\alpha v^2)^{\text{AUSMD}}_{j+1/2} = \frac{1}{2}(\rho\alpha v)_{j+1/2}(v_L + v_R) - \frac{1}{2}|(\rho\alpha v)_{j+1/2}|(v_R - v_L). \tag{70}$$

We note that $\chi_{\text{L}}$ and $\chi_{\text{R}}$ given by (65) and (66) satisfy the relation (40). Consequently, as remarked in Section 4.1, it is easy to check by direct calculation that the AUSMV and AUSMD convective fluxes hold the following property, see also [9, 12].

**Proposition 2.** *The convective fluxes* $(\rho\alpha v)^{\text{AUSMV}}_{j+1/2}$ *and* $(\rho\alpha v)^{\text{AUSMD}}_{j+1/2}$ *are mass coherent in the sense of Definition 1.*

7.3. **WIMF-AUSMD and WIMF-AUSMV.** We are now in a position where we can give a precise definition of fully discrete MF schemes. We shall consider the following two different choices for $(F^A_k)^n$ and $(G^A_k)^n$ leading to two different MF schemes:

**Definition 6.** *We will use the term* **WIMF-AUSMV** *to denote the numerical scheme given by* (47)–(54) *where* $(F^D_k)^{n+1/2}_{j+1/2}$ *is given by the pressure coherent component* (59) *whereas* $(F^A_k)^n_{j+1/2}$ *and* $(G^A_k)^n_{j+1/2}$ *are given by*

$$(F^A_k)^n_{j+1/2} = (\rho\alpha v)^{\text{AUSMV},n}_{k,j+1/2}, \qquad (G^A_k)^n_{j+1/2} = (\rho\alpha v^2)^{\text{AUSMV},n}_{k,j+1/2}$$

**Definition 7.** *We will use the term* **WIMF-AUSMD** *to denote the numerical scheme given by* (47)–(54) *where* $(F^D_k)^{n+1/2}_{j+1/2}$ *is given by the pressure coherent component* (59) *whereas* $(F^A_k)^n_{j+1/2}$ *and* $(G^A_k)^n_{j+1/2}$ *are given by*

$$(F^A_k)^n_{j+1/2} = (\rho\alpha v)^{\text{AUSMD},n}_{k,j+1/2}, \qquad (G^A_k)^n_{j+1/2} = (\rho\alpha v^2)^{\text{AUSMD},n}_{k,j+1/2}$$

The following result holds for WIMF-AUSMV and WIMF-AUSMD:

**Proposition 3.** *WIMF-AUSMV and WIMF-AUSMD satisfy the following properties: (i) The mass fluxes of WIMF-AUSMV and WIMF-AUSMD are mass coherent in the sense of Definition 1. (ii) Both schemes obey Abgrall's principle.*

*Proof.* In view of Lemma 1, result (i) follows directly from Proposition 1 and Proposition 2.

Result (ii) follows by observing that the flux component $G^A_k$ of both schemes (see Definition 6 and 7) satisfy the relation (36) for flow with uniform velocity (35), and then applying Lemma 2. □

**Remark 9.** *We observed in* [9] *that the convective fluxes of AUSMV were considerably more diffusive on volume fraction waves than those of AUSMD. Thus, for numerical simulations we prefer to use the WIMF-AUSMD scheme which applies AUSMD mass and momentum fluxes for* $F^A_k$ *and* $G^A_k$ *respectively. However, we will take advantage of the robustness of the convective fluxes of AUSMV and apply these in combination with the convective fluxes of AUSMD in an appropriate manner when we consider flows which locally involve transition to single-phase flow. We refer to Section 8.3 for details.*

## 8. Numerical Simulations

In the following some selected numerical examples will be presented. We will consider the performance of the WIMF-AUSMD scheme given by Definition 7. In order to ensure that this scheme can handle flow cases which involves transition to single-phase flow, we introduce a slight modification whose purpose basically is to introduce more numerical dissipation near the single-phase zone. This is explained in detail in Section 8.3.

As our main concern will be to demonstrate the inherent accuracy and stability properties of the WIMF-AUSMD scheme, we limit ourselves to first order accuracy in space and time. The boundary conditions are implemented using a simple "ghost cell" approach, where the variables are either imposed or determined by simple (zeroth order) extrapolation from the computational domain.

In the first example we explore more carefully central mechanisms of the WIMF-AUSMD scheme.

8.1. **A Large Relative Velocity Shock.** We consider a Riemann initial value problem investigated by Cortes et al [5] for a similar two-fluid model. Our primary motivation for studying this problem is to investigate the performance of WIMF-AUSMD on sonic waves. The initial states are given by

$$\mathbf{W}_{\mathrm{L}} = \begin{bmatrix} p \\ \alpha_{\mathrm{l}} \\ v_{\mathrm{g}} \\ v_{\mathrm{l}} \end{bmatrix} = \begin{bmatrix} 265000 \text{ Pa} \\ 0.71 \\ 65 \text{ m/s} \\ 1 \text{ m/s} \end{bmatrix} \tag{71}$$

and

$$\mathbf{W}_{\mathrm{R}} = \begin{bmatrix} p \\ \alpha_{\mathrm{l}} \\ v_{\mathrm{g}} \\ v_{\mathrm{l}} \end{bmatrix} = \begin{bmatrix} 265000 \text{ Pa} \\ 0.7 \\ 50 \text{ m/s} \\ 1 \text{ m/s} \end{bmatrix}. \tag{72}$$

8.1.1. *Comparison with explicit scheme.* We here aim to compare the WIMF-AUSMD with an explicit Roe scheme at the same spatial and temporal grid. We refer to [9] for a description of the implementation of the Roe scheme. We assume a grid of 100 cells and use the timestep

$$\frac{\Delta x}{\Delta t} = 400 \text{ m/s}. \tag{73}$$

The results, plotted at the time $t = 0.1$ s, are given in Figure 1. The reference solution was computed using the Roe scheme on a grid of 10 000 cells.

We note that the implicit pressure-momentum coupling used in WIMF-AUMSD causes a stronger numerical dissipation associated with the sonic waves as compared to the explicit Roe scheme whereas the approximation of the volume fraction waves located at about 50 m seem to be very similar. The approximation properties regarding the slow volume fraction waves for WIMF-AUSMD is explored in more detail in the next example (water faucet).

8.1.2. *Test of timestep sensitivity for calculation of pressure using the WIMF-AUSMD scheme.* We now investigate what happens when the timestep is increased beyond the sonic CFL criterion. The two-fluid model possesses an approximate mixture velocity of sound given by (see [30, 9] for details)

$$c = \sqrt{\frac{\rho_{\mathrm{l}}\alpha_{\mathrm{g}} + \rho_{\mathrm{g}}\alpha_{\mathrm{l}}}{\frac{\partial \rho_{\mathrm{g}}}{\partial p}\rho_{\mathrm{l}}\alpha_{\mathrm{g}} + \frac{\partial \rho_{\mathrm{l}}}{\partial p}\rho_{\mathrm{g}}\alpha_{\mathrm{l}}}}. \tag{74}$$

Hence the mixture sound velocity is approximately given by the sound velocity of the gas phase, giving

$$c \approx 317 \text{ m/s}. \tag{75}$$

Hence for timesteps satisfying

$$\frac{\Delta x}{\Delta t} < c, \tag{76}$$

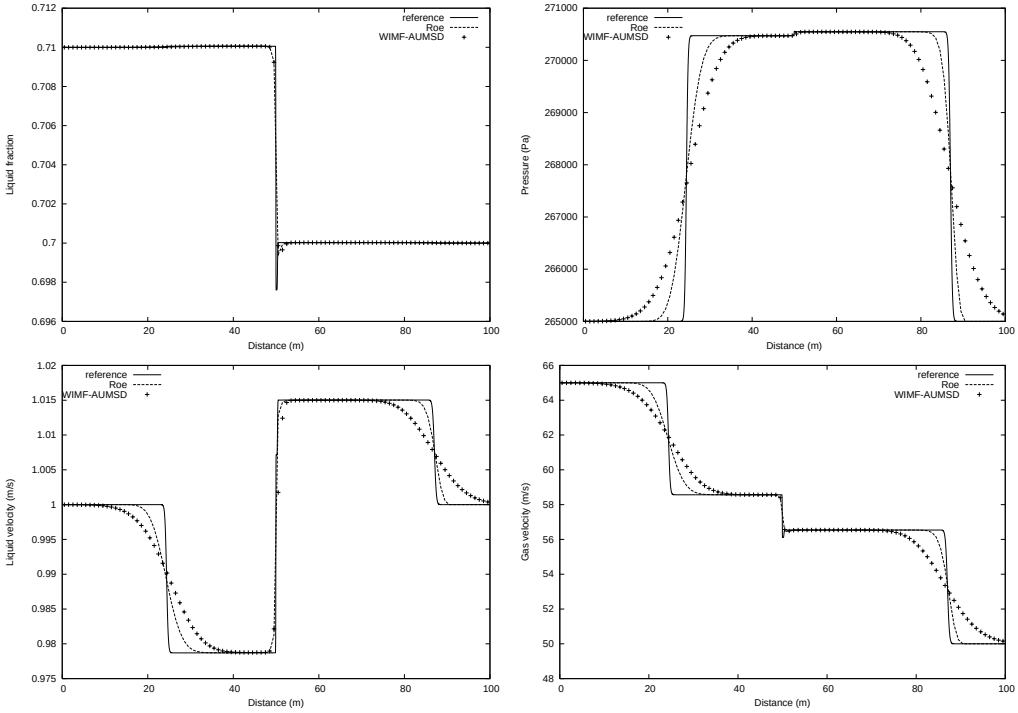


FIGURE 1. LRV shock tube problem. WIMF-AUSMD vs Roe scheme for a grid of 100 cells. Top left: Liquid fraction. Top right: Pressure. Bottom left: Liquid velocity: Bottom right: Gas velocity.

the sonic CFL criterion is broken. For a grid of 1000 cells, the results of the pressure calculation for several different values of $\Delta x/\Delta t$ is given in Figure 2. We observe that increasing the timestep beyond the sonic CFL criterion (2) does not induce instabilities. However, a significant increase of the numerical dissipation of the sonic waves follows the increased timestep.

8.1.3. *Test of stability and convergence for the WIMF-AUSMD scheme under violation of sonic CFL condition.* Using the timestep $\Delta x/\Delta t = 100$ m/s, the effect of grid refinement for the WIMF-AUSMD scheme is demonstrated in Figure 3. We observe that the Roe reference solution is approached in a monotone way and by that verifies that the stability of the WIMF-AUSMD scheme is not governed by the maximal speed of the sonic waves.

8.1.4. *Test of using purely explicit mass fluxes $F_k$.* We now wish to illustrate the need for using the implicitly calculated mass fluxes $I_k^{n+1}$ as given by (59) when we approximate the mass equations. We consider a slight modification of the flux component $F_k^{\mathrm{D}}$ given by (59), where we instead use the momentum from the previous timestep as follows

$$(F_k^D)_{j+1/2}^n = \frac{1}{2}(I_{k,j}^n + I_{k,j+1}^n) + \frac{1}{4}\frac{\Delta x}{\Delta t}(m_{k,j}^n - m_{k,j+1}^n).$$

Results are given in Figure 4 for the timesteps $\Delta x/\Delta t = 1000$ m/s and $\Delta x/\Delta t = 100$ m/s using a grid of 1000 cells. We observe that this works well for $\Delta x/\Delta t = 1000$ m/s when the sonic CFL condition is satisfied. However, increasing the timestep by an order of magnitude leads to CFL-like instabilities, despite the fact that the pressure-momentum coupling still is implicit. It seems to be a crucial step to use information from time level $t^{n+1}$ to achieve stable mass calculations.

**Remark 10.** *In particular, these results illustrate that the combination of using the pressure evolution equation* (49) *and the mixture mass fluxes* (53) *and* (54)*, where* $(F_k^D)^{n+1/2}$ *is given by* (59)*, makes the pressure calculation independent of any sonic CFL condition.*

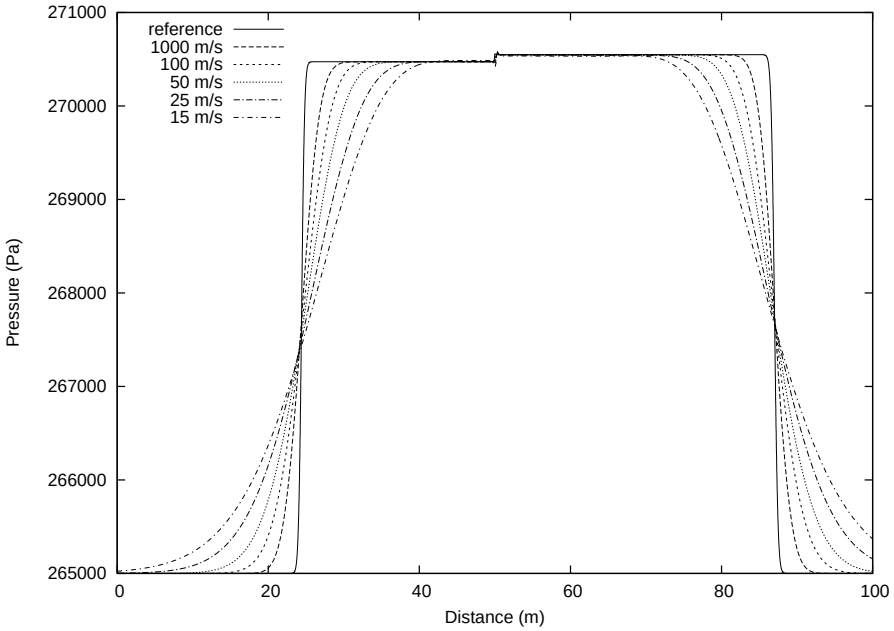


FIGURE 2. LRV shock tube problem. Pressure is shown for a grid of 1000 cells. Different timesteps are considered by considering different values for $\Delta x/\Delta t$ for the WIMF-AUSMD scheme.

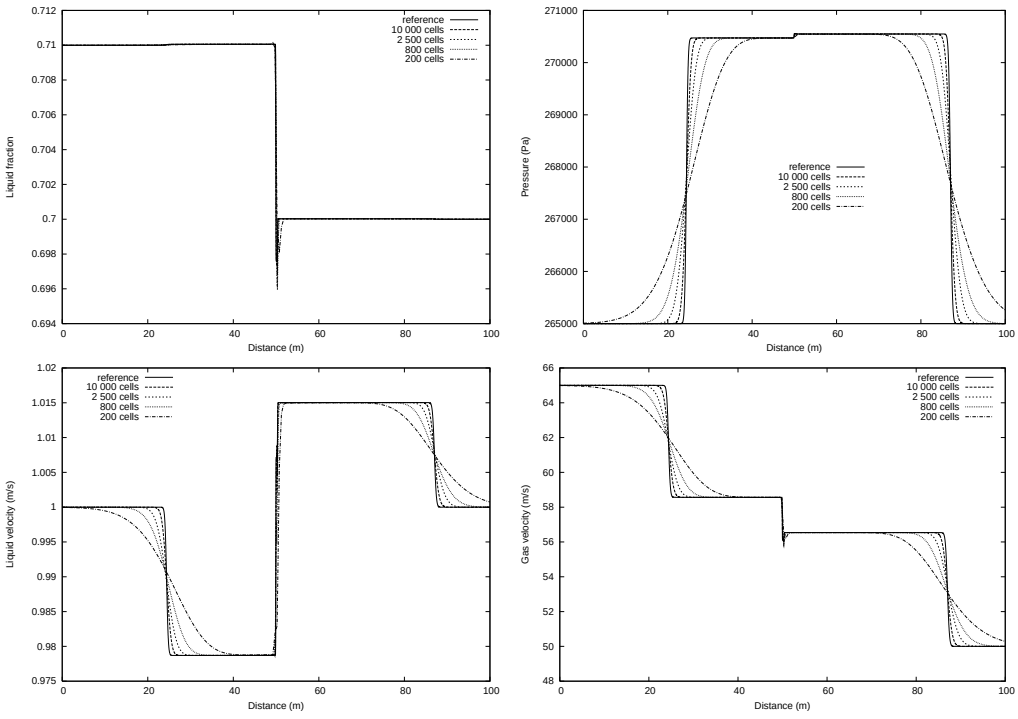


FIGURE 3. LRV shock tube problem. Grid refinement for the WIMF-AUSMD scheme. Top left: Liquid fraction. Top right: Pressure. Bottom left: Liquid velocity. Bottom right: Gas velocity.

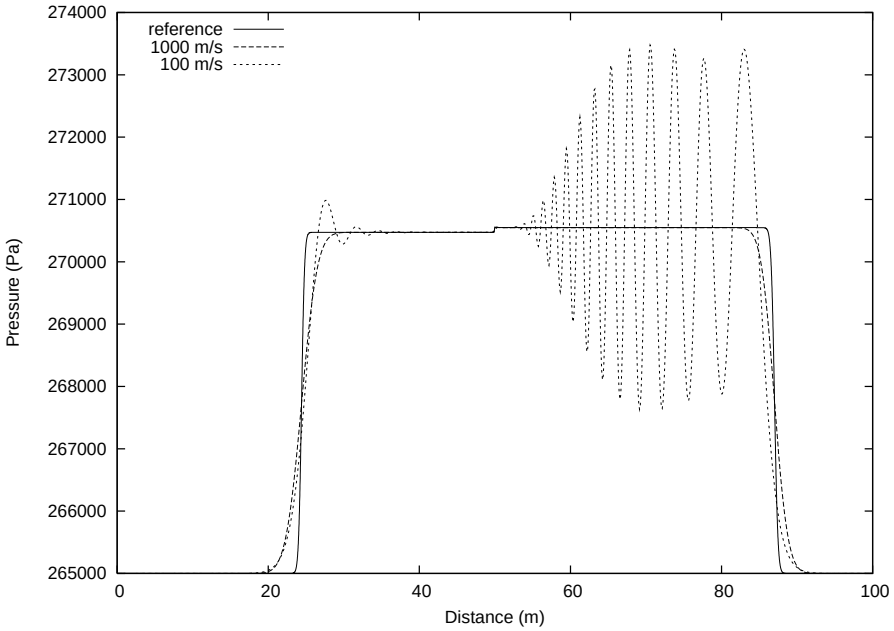


FIGURE 4. LRV shock tube problem, 1000 cells. Modfied WIMF-AUSMD. Purely explicit mass fluxes are used.

The strength of the mixture fluxes (53) and (54) lies in their ability to properly combine the stability of an implicit scheme with the accuracy of an explicit scheme, at least for the resolution of volume fraction waves. This is the central issue in the next example.

8.2. **Water Faucet Problem.** We now wish to focus more on the resolution of volume fraction waves. For this purpose, we study the faucet flow problem of Ransom [22], which has become a standard benchmark [31, 30, 4, 19, 20].

We consider a vertical pipe of length 12 m with the initial uniform state

$$\mathbf{W} = \begin{bmatrix} p \\ \alpha_\mathrm{l} \\ v_\mathrm{g} \\ v_\mathrm{l} \end{bmatrix} = \begin{bmatrix} 10^5 \text{ Pa} \\ 0.8 \\ 0 \\ 10 \text{ m/s} \end{bmatrix}. \tag{77}$$

Gravity is the only source term taken into account, i.e. in the framework of (10) and (11) we have

$$Q_k = g\rho_k\alpha_k, \tag{78}$$

with $g$ being the acceleration of gravity. At the inlet we have the constant conditions $\alpha_\mathrm{l} = 0.8$, $v_\mathrm{l} = 10$ m/s and $v_\mathrm{g} = 0$. At the outlet the pipe is open to the ambient pressure $p = 10^5$ Pa.

We restate the approximate analytical solution presented in the references [20, 31]

$$v_\mathrm{l}(x,t) = \begin{cases} \sqrt{v_0^2 + 2gx} & \text{for } x < v_0 t + \frac{1}{2}gt^2 \\ v_0 + gt & \text{otherwise.} \end{cases} \tag{79}$$

$$\alpha_\mathrm{l}(x,t) = \begin{cases} \alpha_0(1 + 2gxv_0^{-2})^{-1/2} & \text{for } x < v_0 t + \frac{1}{2}gt^2 \\ \alpha_0 & \text{otherwise} \end{cases} \tag{80}$$

where the parameters $\alpha_0 = 0.8$ and $v_0 = 10$ m/s are the initial states.

8.2.1. *Comparison with explicit Roe scheme.* We now compare the WIMF-AUSMD scheme with the explicit Roe scheme under equal conditions. That is, we assume a grid of 120 cells and use the timestep

$$\frac{\Delta x}{\Delta t} = 10^3 \text{ m/s}. \tag{81}$$

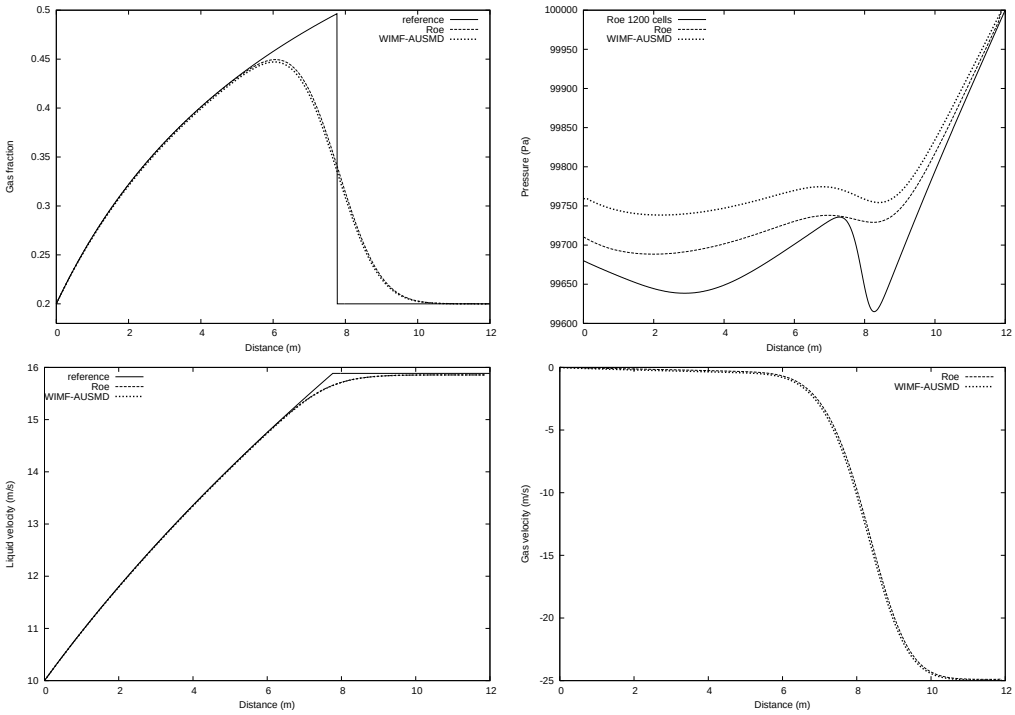


FIGURE 5. Water faucet problem, 120 cells, T=0.6 s. Roe vs WIMF-AUSMD, $\Delta x/\Delta t = 10^3$ m/s. Top left: Gas fraction. Top right: Pressure. Bottom left: Liquid velocity. Bottom right: Gas velocity.

Results are given in Figure 5 after $t = 0.6$ s. We note that there is hardly any visible difference between WIMF-AUSMD and the Roe scheme on the volume fraction wave. However, the WIMF-AUSMD is somewhat more diffusive on pressure. This is consistent with our observations in Section 8.1.1.

8.2.2. *Effect of increasing the timestep for WIMF-AUSMD.* An eigenvalue analysis (see [30, 9]) reveals that the velocities of the volume fraction waves are approximately given by

$$\lambda_{\mathrm{v}}^{\pm} = \frac{\rho_{\mathrm{g}}\alpha_{\mathrm{l}}v_{\mathrm{g}} + \rho_{\mathrm{l}}\alpha_{\mathrm{g}}v_{\mathrm{l}}}{\rho_{\mathrm{g}}\alpha_{\mathrm{l}} + \rho_{\mathrm{l}}\alpha_{\mathrm{g}}} \pm \sqrt{\frac{\Delta p(\rho_{\mathrm{g}}\alpha_{\mathrm{l}} + \rho_{\mathrm{l}}\alpha_{\mathrm{g}}) - \rho_{\mathrm{l}}\rho_{\mathrm{g}}\alpha_{\mathrm{l}}\alpha_{\mathrm{g}}(v_{\mathrm{g}} - v_{\mathrm{l}})^2}{(\rho_{\mathrm{g}}\alpha_{\mathrm{l}} + \rho_{\mathrm{l}}\alpha_{\mathrm{g}})^2}}. \tag{82}$$

For a weakly implicit scheme as defined by (3) we must then have

$$\frac{\Delta x}{\Delta t} \geq \max_{j,n}(\lambda_{\mathrm{v}}^{\pm}). \tag{83}$$

Having $\rho_{\mathrm{l}} >> \rho_{\mathrm{g}}$ we obtain from (82)

$$\lambda_{\mathrm{v}}^{\pm} \approx v_{\mathrm{l}}, \tag{84}$$

hence we expect a weakly implicit scheme to encounter CFL related stability problems near timesteps corresponding to the liquid velocity.

We now study the effect of increasing the timestep for the WIMF-AUSMD scheme. We consider the following timesteps:

- $\Delta x/\Delta t = 1000$ m/s.
- $\Delta x/\Delta t = 25$ m/s.
- $\Delta x/\Delta t = 17$ m/s.
- $\Delta x/\Delta t = 14$ m/s.

Results for these timesteps are given in Figure 6. We observe that increasing the timestep towards

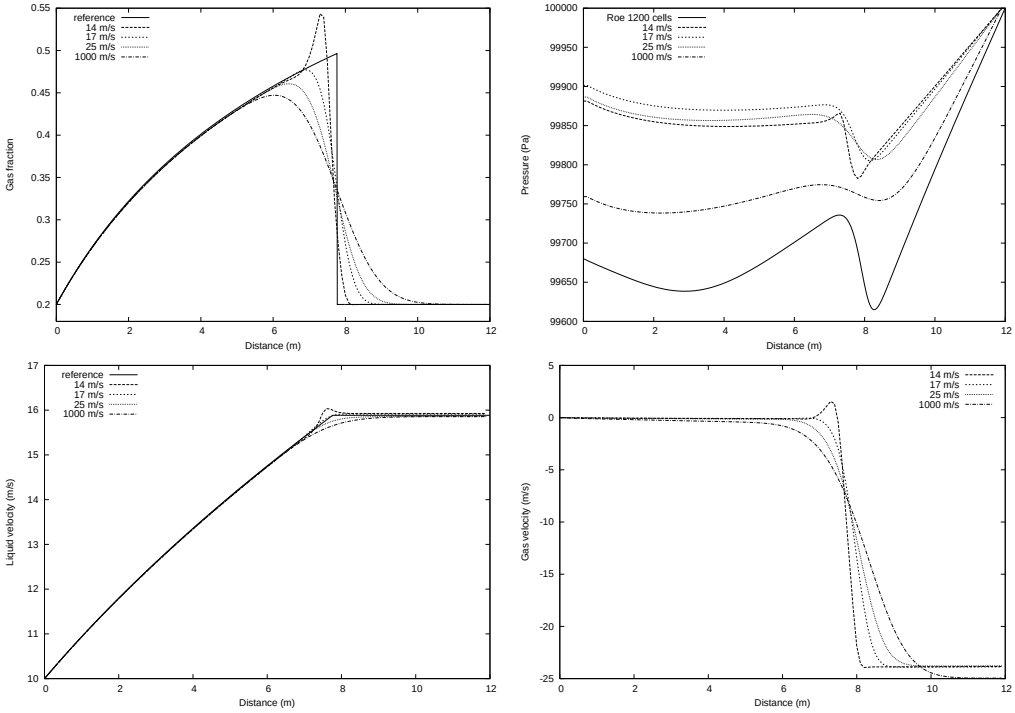


FIGURE 6. Water faucet problem, 120 cells, T=0.6 s. Different timesteps for the WIMF-AUSMD scheme. Top left: Gas fraction. Top right: Pressure. Bottom left: Liquid velocity. Bottom right: Gas velocity.

the timestep corresponding to the liquid velocity significantly improves the accuracy of WIMF-AUSMD on the volume fraction wave, as seen on the plots of velocities and volume fraction. The rate of improvement in accuracy is largest near the optimal timestep $\Delta x/\Delta t = v_{\mathrm{l}}$. Increasing the timestep further violates the weak CFL criterion (83) and instabilities occur. The increased accuracy in volume fraction is accompanied by increased numerical dissipation in the pressure variable, consistent with our observations in Section 8.1.2.

8.2.3. *Optimal WIMF-AUSMD vs Roe scheme.* To emphasize the increased accuracy in volume fraction that is allowed by increasing the timestep beyond the sonic CFL criterion, the explicit Roe scheme at $\Delta x/\Delta t = 1000$ m/s is plotted together with the optimal WIMF-AUSMD scheme ($\Delta x/\Delta t = 17$ m/s) in Figure 7. The improvement of the WIMF-AUSMD scheme is rather striking and is equivalent to an increase in the number of grid cells by an order of magnitude for the Roe scheme.

8.2.4. *Test of convergence for WIMF-AUSMD.* In Figure 8 we investigate how the scheme converges to the expected analytical solution as the grid is refined. The optimal timestep $\Delta x/\Delta t = 17$ m/s is used. As we can see, the expected analytical solution is approached in a nonoscillatory way.

8.3. **Separation Problem.** We consider a gravity-induced phase separation problem introduced by Coquel et al [4], also investigated by Paillère et al [20]. This problem tests the ability of numerical schemes to handle the transition to one-phase flow under stiff conditions.

We assume a vertical pipe of length 7.5 m, where gravitational acceleration and possibly interfacial friction are the source terms taken into account. Initially the pipe is filled with stagnant liquid and gas with a uniform pressure $p_0 = 10^5$ Pa and a uniform liquid fraction $\alpha_{\mathrm{l}} = 0.5$.

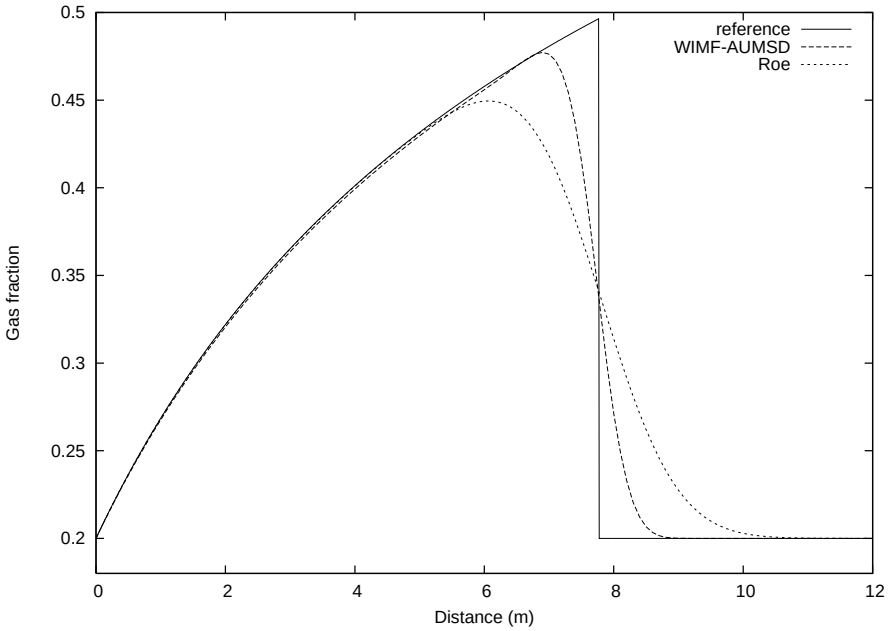


FIGURE 7. Water faucet problem, T=0.6s, 120 grid cells. WIMF-AUSMD with optimal timestep vs explicit Roe scheme.

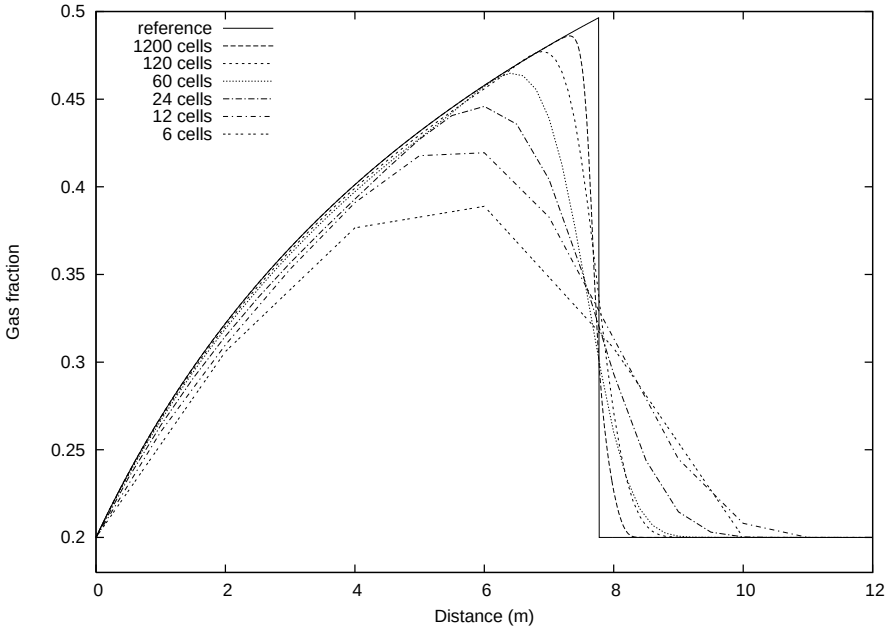


FIGURE 8. Water faucet problem, T=0.6s. Grid refinement for the WIMF-AUSMD scheme.

Assuming that the liquid column falls freely under the influence of gravity, the following approximate analytical solution can be derived for the transient period

$$v_l(x,t) = \begin{cases} \sqrt{2gx} & \text{for } x < \frac{1}{2}gt^2 \\ gt & \text{for } \frac{1}{2}gt^2 \leq x < L - \frac{1}{2}gt^2 \\ 0 & \text{for } L - \frac{1}{2}gt^2 < x \end{cases} \tag{85}$$

$$\alpha_{\rm l}(x,t) = \begin{cases} 0 & \text{for } x < \frac{1}{2}gt^2 \\ 0.5 & \text{for } \frac{1}{2}gt^2 \le x < L - \frac{1}{2}gt^2 \\ 1 & \text{for } L - \frac{1}{2}gt^2 < x \end{cases} \tag{86}$$

where $L = 7.5$ m is the length of the tube. This approximate solution consists of a contact discontinuity at the top of the tube and a shock-like discontinuity at the lower part of the tube. After the time

$$T = \sqrt{\frac{L}{g}} = 0.87 \text{ s} \tag{87}$$

these discontinuities will merge and the phases become fully separated. The volume fraction reach a stationary state, whereas the other variables slowly converge towards a stationary solution. Assuming hydrostatic conditions the pressure will approximately be given by

$$p(x,t) = \begin{cases} p_0 & \text{for } x < L/2 \\ p_0 + \rho_{\rm l} g\,(x - L/2) & \text{for } x \ge L/2. \end{cases} \tag{88}$$

8.3.1. *Transition to one-phase flow.* We observed that the basic WIMF-AUSMD scheme would produce instabilities in the transition to one-phase flow. Indeed this is a common problem for two-phase flow models, observed among others by Coquel et al [4] for their kinetic scheme, Paillére et al [20] for their AUSM$^+$ scheme and Romate [23] for his Roe scheme. Romate suggested a scheme switching strategy for solving this problem, where the original scheme is replaced with a stable, diffusive scheme near one-phase regions. Here we will follow a similar approach, using a strategy that has been previously applied with success [9, 12]. We proceed as follows:

8.3.2. *Modification of basic AUSMV and AUSMD splitting formulas.* We modify the parameters $\chi$ used in the splitting formulas (64) corresponding to the AUSMV and AUSMD schemes as follows

$$\chi_{\rm L} = (1 - \phi_{\rm L})\frac{2(\rho/\alpha)_{\rm L}}{(\rho/\alpha)_{\rm L} + (\rho/\alpha)_{\rm R}} + \phi_{\rm L} \tag{89}$$

and

$$\chi_{\rm R} = (1 - \phi_{\rm R})\frac{2(\rho/\alpha)_{\rm R}}{(\rho/\alpha)_{\rm L} + (\rho/\alpha)_{\rm R}} + \phi_{\rm R} \tag{90}$$

for each phase. Here $\phi$ is the transition fix function

$$\phi = \phi(\alpha_{\rm g}) = e^{-\Gamma_{\rm g}\alpha_{\rm g}} + e^{-\Gamma_{\rm l}(1-\alpha_{\rm g})}, \tag{91}$$

where $\Gamma_k$ is a parameter controlling the diffusive effect of the transition fix. This fix ensures that we recover the more stable FVS/van Leer fluxes, as given by (60)–(63), in one-phase regions.

We observe that the transition to one-phase liquid flow (the denser phase) more easily induces instabilities than the transition to one-phase gas flow (the less dense phase). For the purposes of this paper, we choose the parameters

$$\Gamma_{\rm g} = 50 \tag{92}$$

and

$$\Gamma_{\rm l} = 500. \tag{93}$$

**Definition 8.** *The modified AUSMD scheme as described by* (89) *and* (90) *will be denoted as the AUSMD* scheme. Similarly, the modified AUSMV scheme as described by* (89) *and* (90) *will be denoted as the AUSMV* scheme.*

8.3.3. *WIMF-AUSMDV*.* We consider convective fluxes which are a hybrid of those employed by AUSMD* and AUSMV*, and denoted as AUSMDV*. More precisely, the numerical convective fluxes $(\alpha\rho v)_{j+1/2}$ and $(\alpha\rho v^2)_{j+1/2}$ are given by the following expression:

$$\begin{aligned} (\alpha\rho v)_{j+1/2}^{\rm AUSMDV^*} &= s(\alpha\rho v)_{j+1/2}^{\rm AUSMV^*} + (1-s)(\alpha\rho v)_{j+1/2}^{\rm AUSMD^*} \\ (\alpha\rho v^2)_{j+1/2}^{\rm AUSMDV^*} &= s(\alpha\rho v^2)_{j+1/2}^{\rm AUSMV^*} + (1-s)(\alpha\rho v^2)_{j+1/2}^{\rm AUSMD^*}. \end{aligned} \tag{94}$$

Here $s$ is chosen as

$$s = \max(\phi_{\rm L}, \phi_{\rm R}), \tag{95}$$

where $\phi$ is the transition fix function given by (91). Note that this hybridization only affects the momentum convective fluxes since $(\alpha\rho v)^{\mathrm{AUSMV}^*}_{j+1/2} = (\alpha\rho v)^{\mathrm{AUSMD}^*}_{j+1/2}$. The construction (94) ensures that AUSMDV$^*$ uses the accurate AUSMD$^*$ fluxes in two-phase regions and switches to the more stable AUSMV$^*$ fluxes in one-phase regions.

The WIMF-AUSMDV$^*$ scheme is now constructed straightforwardly by associating the fluxes $F^{\mathrm{A}}_k$ and $G^{\mathrm{A}}_k$ with the corresponding AUSMDV$^*$ fluxes as follows.

**Definition 9.** *We will use the term* **WIMF-AUSMDV**$^*$ *to denote the numerical scheme given by* (47)–(54) *where* $(F^D_k)^{n+1/2}_{j+1/2}$ *is given by the pressure coherent component* (59) *whereas* $(F^A_k)^n_{j+1/2}$ *and* $(G^A_k)^n_{j+1/2}$ *are given by*

$$(F^A_k)^n_{j+1/2} = (\rho\alpha v)^{\mathrm{AUSMDV}^*,n}_{k,j+1/2}, \qquad (G^A_k)^n_{j+1/2} = (\rho\alpha v^2)^{\mathrm{AUSMDV}^*,n}_{k,j+1/2}.$$

**Remark 11.** *The idea of increasing the numerical dissipation near one-phase regions may be explored more systematically with the aim of obtaining more general relations that do not involve free parameters. Paillère et al* [20] *used a related approach, introducing a diffusion term depending on the pressure gradient to improve the performance of their AUSM*$^+$ *scheme near one-phase liquid regions. We stress that the above modified schemes are still fully conservative and consistent with the original basic two-fluid model. In particular the WIMF-AUSMDV*$^*$ *scheme differs from the WIMF-AUSMD scheme only for one-phase regions.*

8.3.4. *Numerical Results.* We now consider two different formulations of the two-fluid model:

- *Frictionless flow.* We assume that gravity is the only source term taken into account. In this case, the lack of friction terms causes the gas velocity to become large as the gas phase is disappearing. We note that for one-phase liquid flow we have $\alpha_{\mathrm{l}} >> \alpha_{\mathrm{g}}$ and the volume fraction velocities (82) are dominated by this large gas velocity. Hence the weak CFL criterion (83) becomes very restrictive here. With this model we use the relatively low timestep
$$\frac{\Delta x}{\Delta t} = 500 \text{ m/s}. \tag{96}$$
For stability of the FVS scheme, which AUSMDV$^*$ employs in the transition to single phase flow, we rescale the sound velocity $c$ as described in the Appendix, using
$$c = 750 \text{ m/s} \tag{97}$$
instead of the sound velocity determined from (16). This choice was based on the fact that we observed that the gas velocity could become as high as approximately 400 m/s. According to (124) in the Appendix, we should then choose $c$ such that $200 \leq c \leq 800$. We consistently have chosen $c$ in the upper region.
- *Interfacial momentum exchange.* The low timestep needed for the frictionless model is undesirable. In addition the assumption of frictionless low is unphysical. In reality we expect the last remnants of the disappearing phase to be completely dissolved, and we expect $v_{\mathrm{g}} \approx v_{\mathrm{l}}$ near one-phase regions. To more realistically model this situation, we consider an interfacial momentum transfer model also used by Paillère et al [20]. For the gas momentum equation, we introduce the source term
$$M^{\mathrm{D}}_{\mathrm{g}} = C\alpha_{\mathrm{g}}\alpha_{\mathrm{l}}\rho_{\mathrm{g}}(v_{\mathrm{g}} - v_{\mathrm{l}}), \tag{98}$$
where $C$ is a positive constant. Likewise the liquid momentum source term is given as
$$M^{\mathrm{D}}_{\mathrm{l}} = -M^{\mathrm{D}}_{\mathrm{g}} = -C\alpha_{\mathrm{g}}\alpha_{\mathrm{l}}\rho_{\mathrm{g}}(v_{\mathrm{g}} - v_{\mathrm{l}}), \tag{99}$$
conserving total momentum. We write
$$C = C_0\phi, \tag{100}$$
making the exchange term kick in more strongly near one-phase regions. Following Paillère et al [20], we set
$$C_0 = 50000 \text{ s}^{-1}. \tag{101}$$

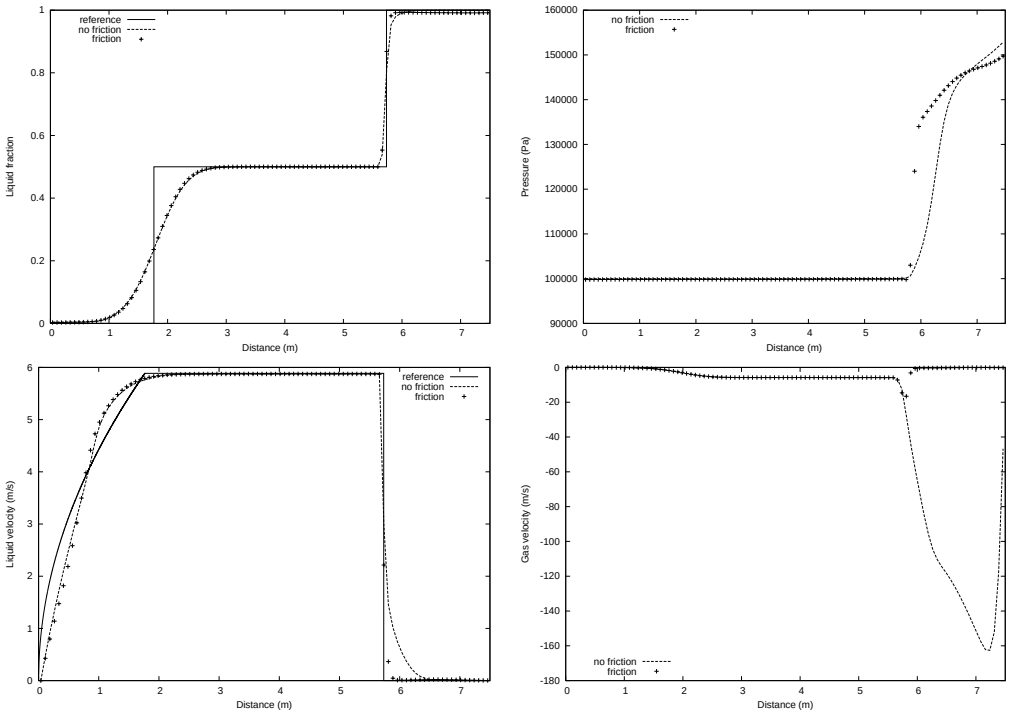


FIGURE 9. Separation problem, T=0.6 s, 100 grid cells. WIMF-AUSMDV* scheme with and without interfacial momentum exchange terms. Top left: Liquid fraction. Top right: Pressure. Bottom left: Liquid velocity. Bottom right: Gas velocity

To avoid stability problems related to stiffness in this term, we use a semi-implicit implementation as follows

$$(M_{\mathrm{g}}^{\mathrm{D}})_j^{n+1/2} = C_j^n (\alpha_{\mathrm{g}}\alpha_{\mathrm{l}}\rho_{\mathrm{g}})_j^n \left[ \frac{(I_{\mathrm{g}})_j^{n+1}}{(m_{\mathrm{g}})_j^n} - \frac{(I_{\mathrm{l}})_j^{n+1}}{(m_{\mathrm{l}})_j^n} \right]. \tag{102}$$

We found that we could now increase the timestep to

$$\frac{\Delta x}{\Delta t} = 75 \text{ m/s}, \tag{103}$$

consistent with the largest gas (volume fraction) velocities during the transient period. The sound velocity is rescaled as

$$c = 150 \text{ m/s}. \tag{104}$$

Again, this choice is based on the criterion (124) where we now can assume that the fluid velocity becomes zero in the transition to single-phase flow (due to the inclusion of the interfacial momentum transfer model). This gives us that $c$ should be chosen in the interval $0 \leq c \leq 2\lambda = 2\Delta x/\Delta t$.

Results after $t = 0.6$ s are plotted in Figure 9, using a grid of 100 cells. The approximate analytical solutions (85) and (86) are used for reference. We note that good accordance with the expected analytical solutions is achieved. The most notable effect of the interfacial momentum exchange term is the reduction of the gas velocity in the one-phase liquid region.

Although the phases will be separated for $t < 1.0$ s, it takes some seconds before the excess momentum has been dissipated at the endpoints. Results for fully stationary conditions ($t = 5.0$ s) are plotted in Figure 10. We note that the frictionless model does not exactly yield the expected hydrostatic pressure distribution. This seems to be due to the strong velocity gradients at the

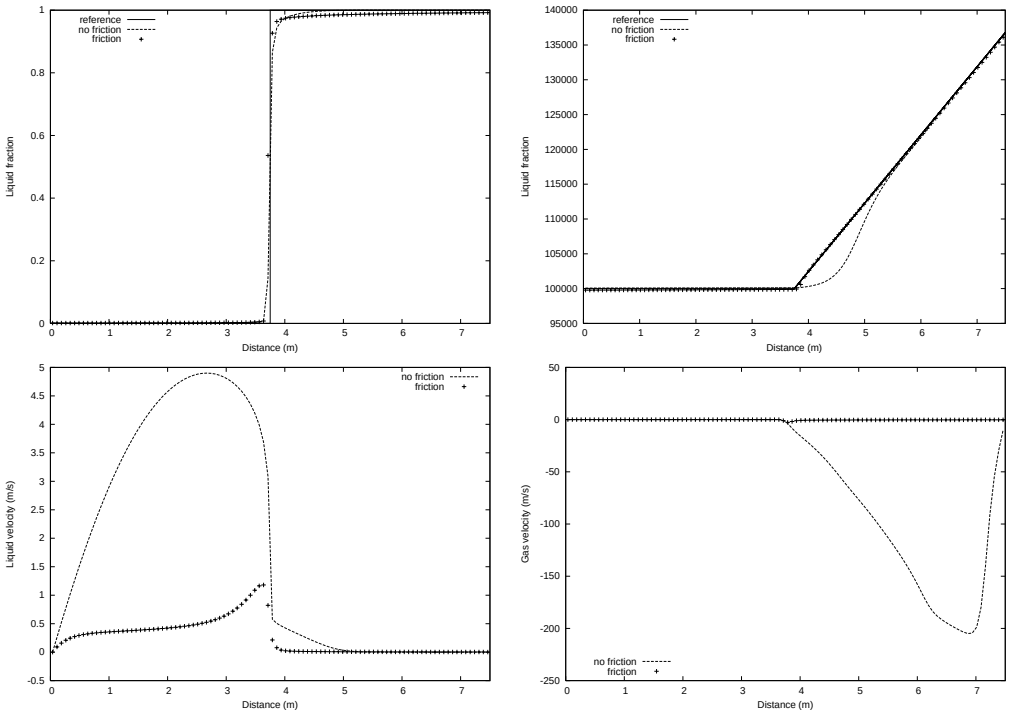


FIGURE 10. Separation problem, $t = 5.0$ s, 100 grid cells. WIMF-AUSMDV* scheme with and without interfacial momentum exchange terms. Top left: Liquid fraction. Top right: Pressure. Bottom left: Liquid velocity. Bottom right: Gas velocity.

separation point, and hydrostatic conditions are never fully reached. The inclusion of the interfacial friction term removes these gradients.

In Figure 11 the effect of grid refinement on the resolution of volume fraction is illustrated for the WIMF-AUSMDV* scheme with momentum exchange terms. The timestep $\Delta x/\Delta t = 75$ m/s is used. The expected analytical solution is approached in a monotone way.

8.4. **Oscillating Manometer Problem.** Finally, we consider a problem introduced by Ransom [22] and investigated by Paillère et al [20] and Evje et al [9]. This problem tests the ability of numerical schemes to handle a change in the flow direction.

We consider a U-shaped tube of total length 20 m. The geometry of the tube is reflected in the $x$-component of the gravity field

$$g_x(x) = \begin{cases} g & \text{for } 0 \le x \le 5 \text{ m} \\ g\cos\left(\frac{(x-5\text{ m})}{10\text{ m}}\pi\right) & \text{for } 5 \text{ m} < x \le 15 \text{ m} \\ -g & \text{for } 15 \text{ m} < x \le 20 \text{ m}. \end{cases} \tag{105}$$

Initally we assume that the liquid fraction is given by

$$\alpha_{\text{l}}(x) = \begin{cases} 10^{-6} & \text{for } 0 \le x \le 5 \text{ m} \\ 0.999 & \text{for } 5 \text{ m} < x \le 15 \text{ m} \\ 10^{-6} & \text{for } 15 \text{ m} < x \le 20 \text{ m}. \end{cases} \tag{106}$$

The initial pressure is assumed to be equal to the hydrostatic pressure distribution. We assume that the gas velocity is uniformly $v_{\text{g}} = 0$, and the liquid velocity distribution is given by

$$v_{\text{l}}(x) = \begin{cases} 0 & \text{for } 0 \le x \le 5 \text{ m} \\ V_0 & \text{for } 5 \text{ m} < x \le 15 \text{ m} \\ 0 & \text{for } 15 \text{ m} < x \le 20 \text{ m}, \end{cases} \tag{107}$$

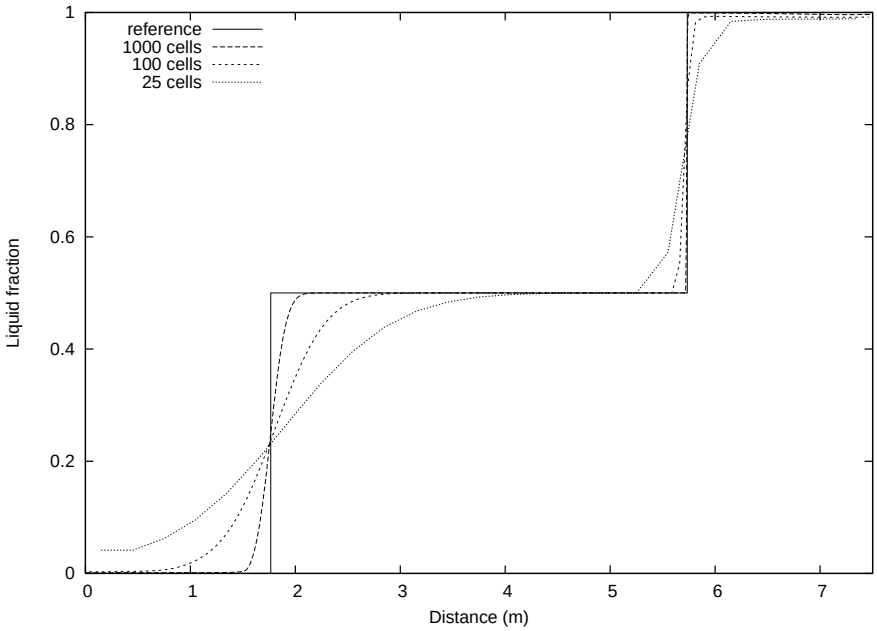


FIGURE 11. Separation problem, T=0.6s. Convergence properties of the WIMF-AUSMDV* scheme with interfacial momentum exchange terms.

where $V_0 = 2.1$ m/s.

Ransom [22] suggested treating the manometer as a closed loop. We will follow the approach of Paillère et al [20], assuming that both ends of the manometer are open to the atmosphere. We assume that the liquid column will move with uniform velocity under the influence of gravity, giving the following approximate analytical solution for the liquid velocity [20]

$$v_l(t) = V_0 \cos(\omega t), \tag{108}$$

where

$$\omega = \sqrt{\frac{2g}{L}} \tag{109}$$

where $L = 10$ m is the length of the liquid column.

In order to exploit the possibility of taking large timesteps, we include the interfacial momentum exchange term as described in Section 8.3.4. The sound velocity is rescaled to $c = 30$ m/s which is consistent with (124) where we use that the fluid velocity becomes zero in the transition to single-phase flow.

8.4.1. *Numerical results.* We consider the following grids

- *100 cells.* We use a timestep corresponding to $\Delta x/\Delta t = 50$ m/s.
- *500 cells.* We use a timestep corresponding to $\Delta x/\Delta t = 15$ m/s.

For the fine grid with 500 cells, the critical timestep was found to be consistent with the weak CFL criterion (83). For the coarse grid consisting of 100 cells, a lower CFL number was needed to ensure stability. The evolution of the center cell liquid velocity is given in Figure 12. We note that the results for 100 and 500 cells are virtually identical, indicating that the resolution of the liquid velocity is not grid sensitive. We observe a slight phase difference from the approximate analytical solution as was also observed in [20, 9].

The distribution of all variables after $t = 20$ s is given in Figure 13 for the grid of 500 cells. We observe that the variables are approximated without any numerical oscillations. In particular there is little numerical diffusion for the volume fraction variable. The strong gradients in the velocities are a consequence of the sudden volume change at the transition points between the

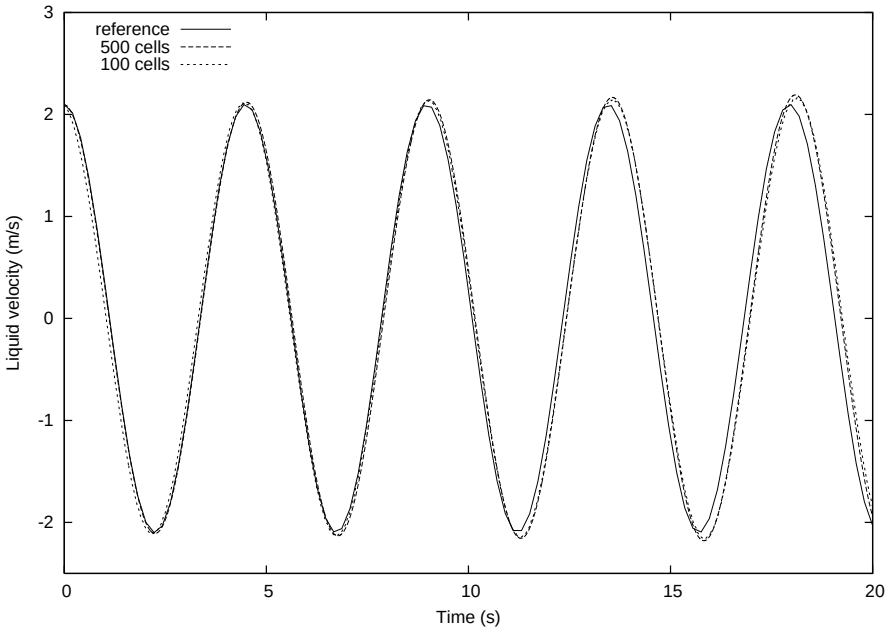


FIGURE 12. Oscillating manometer, WIMF-AUSMDV* scheme. Time development of the liquid velocity.

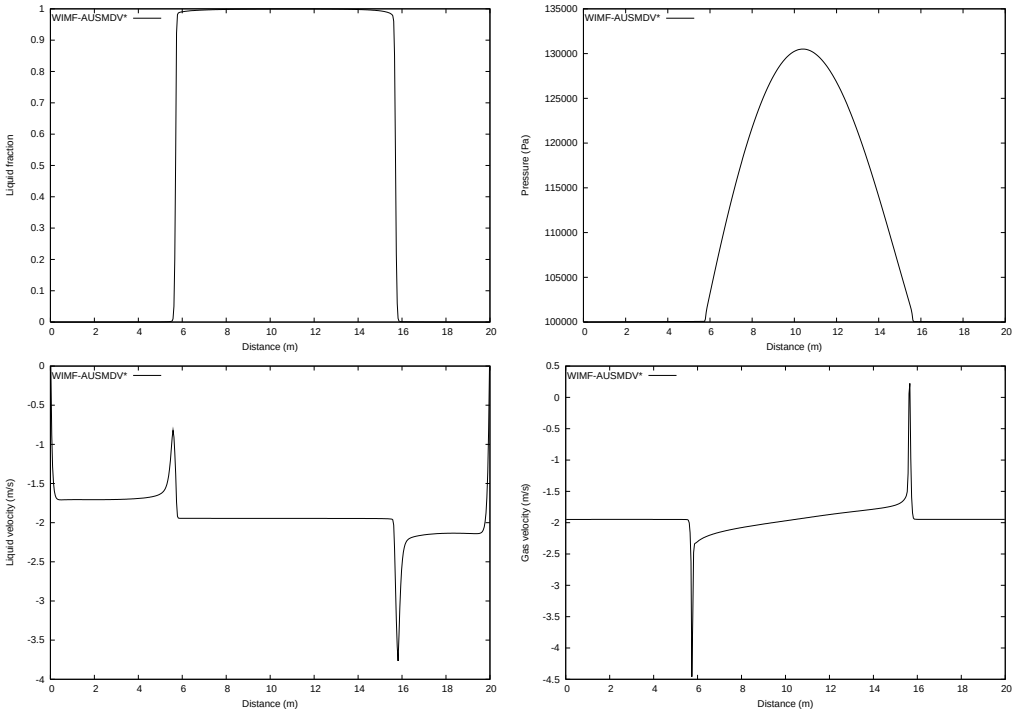


FIGURE 13. Oscillating manometer, t=20.0 s, 500 grid cells. WIMF-AUSMDV* scheme. Top left: Liquid fraction. Top right: Pressure. Bottom left: Liquid velocity. Bottom right: Gas velocity

phases. We remark that the gas velocity was extrapolated at the boundaries, whereas the liquid velocity was forced to zero at the boundaries to avoid liquid mass leakage.

## 9. Summary

We have proposed a general framework for constructing weakly implicit methods for the two-fluid model. Particularly, we have constructed a weakly implicit numerical scheme, denoted as WIMF-AUSMD, that allows the CFL criterion for sonic waves to be violated. All the numerical experiments indicate that a weaker CFL criterion applies with relation to the slow-moving volume fraction waves.

The scheme is based on a previously developed "Mixture Flux" approach [12] which properly combines diffusive and nondissipative fluxes to yield an accurate and robust resolution of sonic and volume fraction waves on nonstaggered grids. The sonic CFL criterion is violated by enforcing a coupling between the "pressure wave" component of the mixture flux, the cell center momenta and the cell interface pressure. In particular all convective (mass and momentum) fluxes are treated in an explicit manner. Hence we believe that higher order versions of the scheme may be implemented, for instance by using the MUSCL technique of van Leer [7, 14].

The numerical evidence indicates that the WIMF-AUSMD is highly robust and efficient, and gives an accuracy potentially superior to the explicit Roe scheme on volume fraction waves. An added advantage of the WIMF-AUSMD scheme is that it does not require a full eigenstructure decomposition of the jacobi matrix for the system. However, the scheme is diffusive on pressure waves, especially for large timesteps.

By increasing the numerical dissipation near one-phase regions, we have demonstrated that the framework allows for accurate, efficient and robust solutions also for flow cases which locally involve the transition from one-phase to two-phase flow.

**Acknowledgements.** The second author thanks the Norwegian Research Council for financial support through the Petronics program.

## References

[1] R. Abgrall, How to prevent pressure oscillations in multicomponent flow calculations, *J. Comput. Phys.* **125**, 150–160, 1996.
[2] F. Barre et al. The cathare code strategy and assessment. *Nucl. Eng. Des.* **124**, 257–284, 1990.
[3] K. H. Bendiksen, D. Malnes, R. Moe, and S. Nuland, The dynamic two-fluid model OLGA: Theory and application, in *SPE Prod. Eng.* **6**, 171–180, 1991.
[4] F. Coquel, K. El Amine, E. Godlewski, B. Perthame, and P. Rascle, A numerical method using upwind schemes for the resolution of two-phase flows, *J. Comput. Phys.* **136**, 272–288, 1997.
[5] J. Cortes, A. Debussche, and I. Toumi, A density perturbation method to study the eigenstructure of two-phase flow equation systems, *J. Comput. Phys.* **147**, 463–484, 1998.
[6] J. R. Edwards, R. K. Franklin, and M.-S. Liou, Low-diffusion flux-splitting methods for real fluid flows with phase transition, *AIAA Journal* **38**, 1624-1633, 2000.
[7] S. Evje and K. K. Fjelde, Hybrid flux-splitting schemes for a two-phase flow model, *J. Comput. Phys.* **175**, 674–701, 2002.
[8] S. Evje and K. K. Fjelde, On a rough ausm scheme for a one-dimensional two-phase flow model, *Comput. & Fluids* **32**, 1497–1530, 2003.
[9] S. Evje and T. Flatten, Hybrid flux-splitting schemes for a common two-fluid model, *J. Comput. Phys*, to appear.
[10] I. Faille and E. Heintzé, A Rough Finite Volume Scheme for Modeling Two-Phase Flow in a Pipeline, *Computers & Fluids* **28**, 213–241, 1999.
[11] K.-K. Fjelde and K.H. Karlsen, High-resolution hybrid primitive-conservative upwind schemes for the drift flux model, *Comput. & Fluids* **31**, 335–367, 2002.
[12] T. Flatten and S. Evje, A Mixture Flux Approach for Accurate and Robust Reolution of Two-Phase Flows, *Submitted*, July 2003.
[13] M. Larsen, E. Hustvedt, P. Hedne, and T. Straume. Petra: A novel computer code for simulation of slug flow. In *SPE Annual Technical Conference and Exhibition*. Society of Petroleum Engineers, October 1997. SPE 38841.
[14] B. V. Leer, Towards the ultimate conservative difference scheme. V. a second-order sequel to godunov's method, *J. Comput. Phys.* **32**, 101–136, 1979.
[15] M.-S. Liou, A sequel to AUSM: AUSM(+), *J. Comput. Phys.* **129**, 364–382, 1996.

[16] J. M. Masella, Q. H. Tran, D. Ferre and C. Pauchon, Transient simulation of two-phase flow in pipes, *Int. J. Multiphase Flow* **24**,739–755, 1998.
[17] J. M. Masella, I. Faille, and T. Gallouet, On an approximate godunov scheme, *Int. J. Comput. Fluid. Dyn.*, 12:133–149, 1999.
[18] Y. Y. Niu, Simple conservative flux splitting for multi-component flow calculations, *Num. Heat Trans.* **38**, 203-222, 2000.
[19] Y.-Y. Niu, Advection upwinding splitting method to solve a compressible two-fluid model, *Int. J. Numer. Meth. Fluids* **36**, 351–371, 2001.
[20] H. Paillère, C. Corre and J.R.G Cascales, On the extension of the AUSM+ scheme to compressible two-fluid models, *Comput. & Fluids* **32**, 891–916, 2003.
[21] C. Pauchon, H. Dhulesia, D. Lopez and J. Fabre, TACITE: A Comprehensive Mechanistic Model for Two-Phase Flow, *BHRG Conference on Multiphase Production*, Cannes, June 1993.
[22] V. H. Ransom, Numerical bencmark tests, *Multiphase Sci. Tech.* **3**, 465-473, 1987.
[23] J. E. Romate, An approximate riemann solver for a two-phase flow model with numerically given slip relation, *Comput. & Fluids* **27**, 455–477, 1998.
[24] R. Saurel and R. Abgrall, A multiphase godunov method for compressible multifluid and multiphase flows, *J. Comput. Phys.* **150**, 425–467, 1999.
[25] R. Saurel and R. Abgrall, A simple method for compressible multifluid flows, *SIAM J. Sci. Comp.* **21**, 1115–1145, 1999.
[26] H. B. Stewart and B. Wendroff, Review article; two-phase flow: Models and methods, *J. Comput. Phys.* **56**, 363–409, 1984.
[27] I. Tiselj and S. Petelin, Modelling of two-phase flow with second-order accurate scheme, *J. Comput. Phys.* **136**, 503–521, 1997.
[28] E. Tadmor, Numerical viscosity and the entropy condition for conservative difference schemes, *Math. Comp.* **43**,369–381, 1984.
[29] I. Toumi, An upwind numerical method for two-fluid two-phase flow models, *Nuc. Sci. Eng.* **123**, 147–168, 1996.
[30] I. Toumi and A. Kumbaro, An approximate linearized riemann solver for a two-fluid model, *J. Comput. Phys.* **124**, 286–300, 1996.
[31] J. A. Trapp and R. A. Riemke, A nearly-implicit hydrodynamic numerical scheme for two-phase flows, *J. Comput. Phys.* **66**, 62–82, 1986.
[32] Y. Wada and M.-S. Liou, An accurate and robust flux splitting scheme for shock and contact discontinuities, *SIAM J. Sci. Comput.* **18**, 633–657, 1997.

## Appendix

**Rescaling the Sound Velocity.** A problem with the original FVS scheme is that it can produce instabilities for large timesteps if the discretization parameter $\lambda = \Delta x/\Delta t$ is chosen much smaller than the sound velocity. For an explicit scheme this will never be a problem as the CFL criterion limits the timesteps we can take. For a semi-implicit method however, we wish to use a value for $\lambda$ that may be several orders of magnitude smaller than the physical sound velocity and the issue becomes of relevance. To describe the problem, we consider the mass conservation equation

$$\frac{\partial u}{\partial t} + \frac{\partial (uv)}{\partial x} = 0 \tag{110}$$

where $u = \rho_k \alpha_k$. We now consider the FVS scheme

$$(uv)_{j+1/2} = V^+(v_j, c)u_j + V^-(v_{j+1}, c)u_{j+1}. \tag{111}$$

where we use the splitting formulas (60), assuming $v < c$

$$V^{\pm}(v, c) = \pm \frac{1}{4c}(v \pm c)^2. \tag{112}$$

**Total Variation Stability.** We now take advantage of the following theorem due to Harten, as stated by Tadmor [28]

**Theorem 1.** *Consider the scalar equation*

$$\frac{\partial u}{\partial t} + \frac{\partial f(u)}{\partial x} = 0 \tag{113}$$

*solved by the numerical scheme*

$$\frac{u_j^{n+1} - u_j}{\Delta t} + \frac{1}{\Delta x}\left(F(u_j^n, u_{j+1}^n) - F(u_{j-1}^n, u_j^n)\right) = 0 \tag{114}$$

*where the numerical flux $F(u_j^n, u_{j+1}^n)$ is written on viscous form*

$$F_{j+1/2} = F(u_j^n, u_{j+1}^n) = \frac{1}{2}\left(f(u_j^n) + f(u_{j+1}^n)\right) - \frac{1}{2}\frac{\Delta x}{\Delta t} Q_{j+1/2}^n (u_{j+1}^n - u_j^n). \tag{115}$$

*The scheme (114) is total variation nonincreasing provided its numerical viscosity coefficient $Q_{j+1/2}^n = Q(u_j^n, u_{j+1}^n)$ satisfies*

$$\frac{\Delta t}{\Delta x}\left|\frac{f(u_{j+1}^n) - f(u_j^n)}{u_{j+1}^n - u_j^n}\right| \leq Q_{j+1/2}^n \leq 1. \tag{116}$$

For the scheme (111) using the splitting formulas (112) we obtain the numerical viscosity coefficient

$$Q_{j+1/2}^n = \frac{\Delta t}{\Delta x}\frac{v^2 + c^2}{2c}. \tag{117}$$

Using this and assuming uniform velocity we can write the requirement (116) as

$$\frac{\Delta t}{\Delta x} v \leq \frac{\Delta t}{\Delta x}\frac{v^2 + c^2}{2c} \leq 1, \tag{118}$$

which yields the following lemma

**Lemma 3.** *Let the mass equation (110) be solved using the numerical fluxes given by (111) and (112). Then the resulting scheme is total variation nonincreasing if*

$$\frac{\Delta x}{\Delta t} \geq \frac{v^2 + c^2}{2c} \tag{119}$$

*and*

$$c > 0. \tag{120}$$

*The criterion (119) attains its minimum value for $v = c$, for which we obtain*

$$\frac{\Delta x}{\Delta t} \geq v, \tag{121}$$

*which is the standard CFL criterion.*

To further investigate how $c$ should be chosen, we now assume that

$$\lambda = \frac{\Delta x}{\Delta t} \tag{122}$$

is known and investigate which criteria govern the possible choices for $c$. From (119) we obtain

$$c^2 - 2c\lambda + v^2 \leq 0. \tag{123}$$

Solving this equation we obtain the following corollary

**Corollary 1.** *Let the linear advection equation (110) be solved using the numerical fluxes given by (111) and (112). Assume the timestep $\lambda = \Delta x/\Delta t$ is known. Then the resulting scheme is total variation nonincreasing if the "sound velocity" $c$ satisfies*

$$\lambda - \sqrt{\lambda^2 - v^2} \leq c \leq \lambda + \sqrt{\lambda^2 - v^2}. \tag{124}$$

This result is confirmed by numerical experiments and illustrates that if $c >> \lambda$ the FVS scheme is unstable. We hence propose to rescale the sound velocity used in the flux-splitting schemes such that the requirement (124) is satisfied also for large timesteps. We stress that this step is necessary to achieve stability on the *advective* effects for the FVS scheme. Stability of the *sonic* waves is an independent problem that we wish to achieve through taking advantage of the implicit pressure-momentum coupling together with the decomposition of $F_k$ into $F_k^D$ and $F_k^A$.